

RESEARCH ARTICLE

A nuclear export sequence promotes CRM1-dependent targeting of the nucleoporin Nup214 to the nuclear pore complex

Mohamed Hamed, Birgit Caspar, Sarah A. Port* and Ralph H. Kehlenbach[‡]

ABSTRACT

Nup214 is a major nucleoporin on the cytoplasmic side of the nuclear pore complex with roles in late steps of nuclear protein and mRNA export. It interacts with the nuclear export receptor CRM1 (also known as XPO1) via characteristic phenylalanine-glycine (FG) repeats in its C-terminal region. Here, we identify a classic nuclear export sequence (NES) in Nup214 that mediates Ran-dependent binding to CRM1. Nup214 versions with mutations in the NES, as well as wild-type Nup214 in the presence of the selective CRM1 inhibitor leptomycin B, accumulate in the nucleus of Nup214-overexpressing cells. Furthermore, physiological binding partners of Nup214, such as Nup62 and Nup88, are recruited to the nucleus together with Nup214. Nuclear export of mutant Nup214 can be rescued by artificial nuclear export sequences at the C-terminal end of Nup214, leading also to a correct localization of Nup88. Our results suggest a function of the Nup214 NES in the biogenesis of the nuclear pore complex and/or in terminal steps of CRM1-dependent protein export.

KEY WORDS: Nup214, Nup88, CRM1, Nuclear pore complex, Nuclear export sequence

INTRODUCTION

CRM1 (also known as exportin 1, XPO1) is the best-characterized nuclear export receptor, with several hundred identified cargo proteins (Kırlı et al., 2015; Mackmull et al., 2017; Thakar et al., 2013; Wühr et al., 2015). These cargoes typically contain a short sequence motif, a nuclear export sequence (NES) with characteristic hydrophobic residues occurring with a somewhat flexible spacer length, which is recognized by CRM1. Particularly prominent among these motifs is the so-called class 1a NES (Kosugi et al., 2008), which has the characteristic sequence $(\phi_0xx)\phi_1xxx\phi_2xx\phi_3x\phi_4$, where ϕ is a hydrophobic amino acid residue and x is any amino acid. ϕ_0 was identified as an additional hydrophobic residue that can lead to CRM1 binding with particularly high affinity (Güttler et al., 2010). CRM1 belongs to a family of nuclear transport receptors (NTRs) with importin β as the founding member (Fried and Kutay, 2003; Hutten and Kehlenbach, 2007). All these NTRs interact with the GTP-bound form of Ran, a 25 kDa protein that determines the directionality of nuclear transport. In nuclear export, RanGTP is required for the formation of an exportin (e.g. CRM1)–cargo complex in the nucleus. In nuclear import, by contrast, nuclear RanGTP dissociates incoming

importin (e.g. importin β)–cargo complexes. A high concentration of nuclear RanGTP results from dedicated import of RanGDP into the nucleus by the transport factor NTF2 (Ribbeck et al., 1998), followed by GDP–GTP exchange as catalyzed by chromatin-bound RCC1 (Bischoff and Ponstingl, 1991). In the cytoplasm, on the other hand, RanGAP (RANGAP1; Bischoff et al., 1995a), together with RanBP1 (Bischoff et al., 1995b) promote GTP hydrolysis of Ran. Importin and exportin transport complexes are able to pass the permeability barrier of the nuclear pore complex (NPC), because NTRs engage in multiple interactions with phenylalanine-glycine (FG)-repeat regions of nucleoporins, the building blocks of the NPC. For CRM1, a functional interaction with Nup214, a nucleoporin that is found on the cytoplasmic side of the NPC (Kraemer et al., 1994), has been identified (Hutten and Kehlenbach, 2006; Kehlenbach et al., 1999). More recently, we also described the interaction of CRM1 with the FG repeats of Nup214 at a biochemical and a structural level (Port et al., 2015; Roloff et al., 2013). At least eight hydrophobic pockets in N- and C-terminal regions of CRM1 participate in binding to FG motifs of Nup214, resulting in a particularly tight interaction. Nevertheless, rapid dissociation rates are required as well, in order to allow fast transport kinetics. Single molecule approaches have shed light on the peculiar mechanisms that govern the interaction of CRM1 with Nup214 (Tan et al., 2018).


The Nup214 protein is characterized by an N-terminal seven-bladed β -propeller region (Napetschnig et al., 2007), a central coiled-coil region and a C-terminal region that is very rich in FG-repeats (Fig. 1A). The *Nup214* gene was originally identified in the context of chromosomal translocations occurring in certain leukemias (von Lindern et al., 1990) that lead to aberrant fusion proteins (von Lindern et al., 1992a,b,c). Such oncogenic proteins, which contain the C-terminal, FG-rich region of Nup214, were shown to form dynamic nuclear bodies and to inhibit CRM1-dependent nuclear export (Oka et al., 2010; Port et al., 2016). At its physiological localization, the NPC, Nup214 interacts with Nup62 and Nup88, probably forming a trimeric complex by interactions of the coiled-coil regions of the individual proteins (Hampeolz et al., 2019). This has been described in some detail for the yeast homologs of Nup62, Nup88 and Nup214, namely Nsp1, Nup82 and Nup159 (Belgareh et al., 1998; Grandi et al., 1995). In yeast, this Nup82 complex has also been analyzed at a structural level, revealing a P-shaped assembly of proteins (Gaik et al., 2015) that may position the FG repeats of Nsp1 and Nup159 towards the central channel of the NPC (Fernandez-Martinez et al., 2016).

Nup214 has been implicated in late steps of CRM1-dependent nuclear export, affecting certain protein cargoes more than others (Bernad et al., 2006; Hutten and Kehlenbach, 2006). It also plays an important role in mRNA export, as it serves as a binding site for the transport factor NXF1 (Bachi et al., 2000; Katahira et al., 1999) and the RNA helicase Dbp5 (also known as DDX19; Napetschnig et al., 2009; von Moeller et al., 2009).

Department of Molecular Biology, Faculty of Medicine, GZMB, Georg-August-University Göttingen, Humboldtallee 23, 37073 Göttingen, Germany.

*Present address: Department of Molecular Biology, Princeton University, Washington Rd, Princeton, NJ 08544, USA.

[‡]Author for correspondence (rkehlen@gwdg.de)

 S.A.P., 0000-0002-1897-0510; R.H.K., 0000-0003-4920-9916

Handling Editor: Maria Carmo-Fonseca
Received 4 December 2020; Accepted 2 February 2021

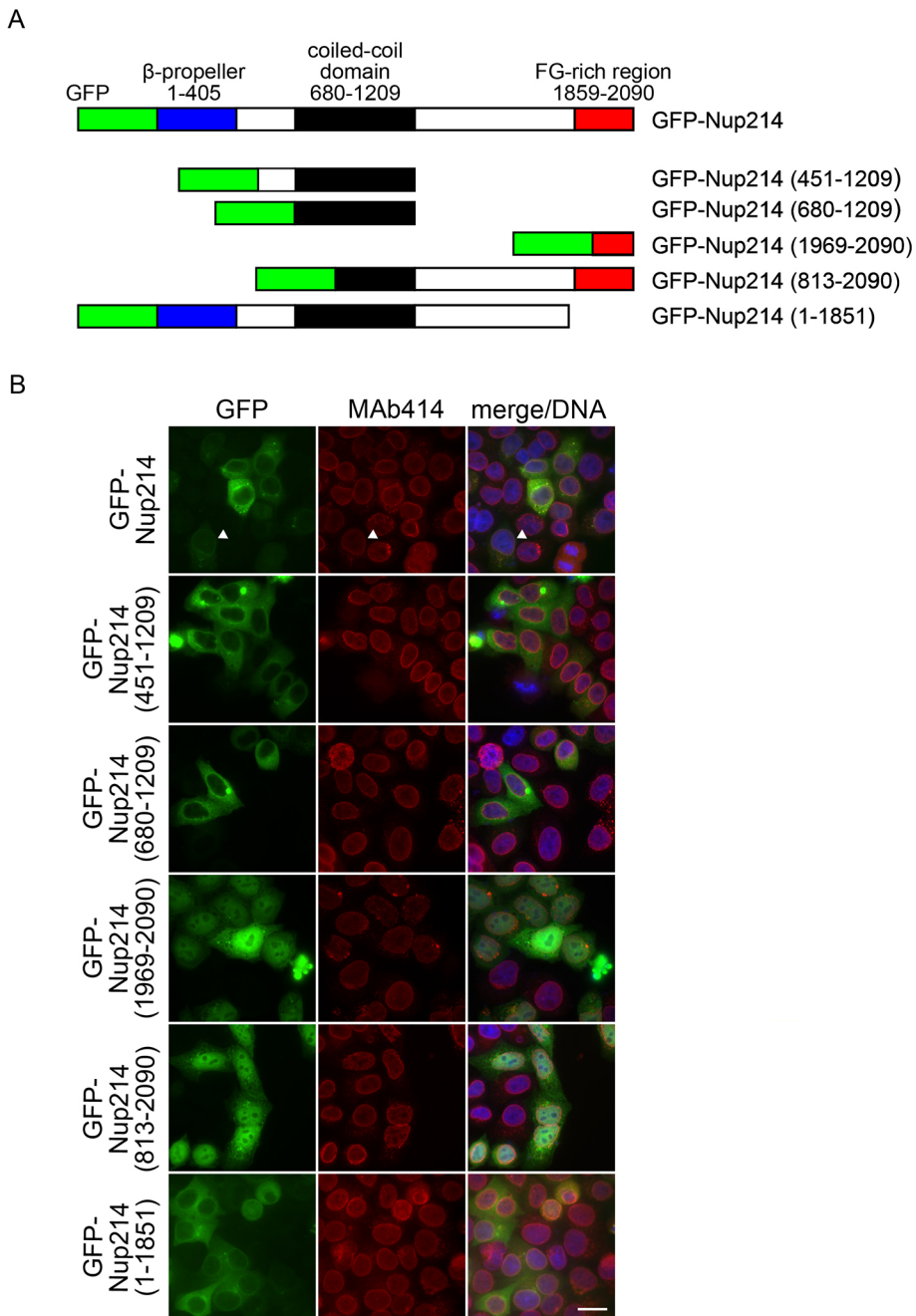


Fig. 1. Nup214 domains show different localization patterns. (A) Schematic representation of GFP-tagged full-length Nup214 and the indicated Nup214 fragments. The β propeller, coiled-coil domain and FG-rich region are indicated, with amino acid numbers shown. (B) Representative images of cells expressing GFP-tagged proteins as shown in A. HeLa cells were transfected with plasmids coding for the indicated GFP-tagged Nup214 fragments and subjected to indirect immunofluorescence using the Mab414 antibody to detect FG-containing nucleoporins. DNA was stained with DAPI (blue), and the cells were analyzed by fluorescence microscopy. Arrowheads, cells expressing low levels of full-length GFP-Nup214. Images are representative of three experiments. Scale bar: 20 μ m.

The NPC as a whole is a very large protein complex with ~30 different nucleoporins that occur in multiples of eight. Many of them assemble into discrete subcomplexes like the Nup214–Nup88–Nup62 complex. In recent years, the biogenesis of the NPC has been investigated in some detail. There are two conceptually very different pathways leading to the formation of novel NPCs (reviewed in Otsuka and Ellenberg, 2018; Weberruss and Antonin, 2016). The postmitotic pathway becomes active at the end of mitosis, after endoplasmic reticulum membrane sheets cover the condensed chromosomes in anaphase. The nucleoporin ELYS (also known as AHCTF1) is the first nucleoporin to bind to chromatin (Doucet et al., 2010; Franz et al., 2007; Rasala et al., 2006), followed by recruitment of several NPC subcomplexes. The cytoplasmic nucleoporins – and Nup214 in particular – have been shown to insert into novel pores at a rather late stage of biogenesis

(Dultz et al., 2008), possibly even in early G1, when the permeability barrier of the NPC has already been established. The second pathway occurs during interphase, when the cell and its nucleus grow and the number of nuclear pores roughly doubles before the next cell division (D'Angelo et al., 2006; Dultz and Ellenberg, 2010). Similar to the postmitotic pathway, cytoplasmic nucleoporins, including Nup214, seem to be added to the novel pore at a very late stage of biogenesis (Otsuka et al., 2016). Besides a complete *de novo* synthesis, a partial exchange of individual nucleoporins can also be envisioned. In this scenario, individual nucleoporins seem to have very different lifetimes; whereas the scaffold nucleoporins, which link the NPC to the nuclear envelope, are extremely long-lived, the nucleoporins of the central channel and also the peripheral nucleoporins like Nup214 are exchanged more rapidly (Savas et al., 2012; Toyama et al., 2019). The

mechanisms for nucleoporin exchange within existing and functional NPCs have not been investigated in detail so far.

Here, we describe the identification of a functional NES in Nup214. CRM1-dependent export of nuclear Nup214 and/or CRM1-dependent binding of newly synthesized Nup214 to the cytoplasmic side of the NPC may promote the incorporation of the nucleoporin into novel or preexisting nuclear pore complexes.

RESULTS

Nup214 contains a CRM1-dependent NES

Endogenous Nup214 typically localizes to the nuclear envelope (NE), specifically to the cytoplasmic side of the NPC (Kraemer et al., 1994). Transfection of cells with constructs coding for either full-length Nup214 or fragments of the nucleoporin, however, can lead to different subcellular targeting of the overexpressed proteins, resulting in NE, nuclear or cytoplasmic localization (Boer et al., 1998; Fornerod et al., 1995, 1996; Napetschnig et al., 2009; Roloff et al., 2013). Fragments containing the N-terminal region and/or the coiled-coil region of Nup214 tend to associate with other proteins of the NPC. By contrast, fragments containing mainly the C-terminal region of Nup214 accumulate in the nucleus. This nuclear accumulation has been attributed to a high prevalence of FG repeats in this part of the protein, which facilitate passage across the permeability barrier of the NPC.

We investigated the localization of full-length Nup214 and fragments thereof (Fig. 1A), focusing on a potential localization to cytoplasmic regions. At low levels of expression, GFP–Nup214 (1–2090), the full-length protein, was found at the NE, as expected (Fig. 1B). At higher expression levels, the protein was also found in the cytoplasm, probably resulting from saturation of potential binding sites at the NE. In part, the protein occurred as ‘cytoplasmic dots’ in such cells, suggesting the formation of larger complexes or aggregates. A short fragment from the C-terminal end [GFP–Nup214 (1969–2090)], which contains the FG-rich region, was largely nuclear, confirming previous results (Fornerod et al., 1996). Other fragments showed either a cytoplasmic localization with occasional nuclear rims [GFP–Nup214 (451–1209) and GFP–Nup214 (680–1209)] or a mixed localization [GFP–Nup214 (831–2090)]. A fragment lacking the FG-rich region [GFP–Nup214 (1–1851)] was largely excluded from the nucleus, with a nuclear rim being visible in many cells. These results raised the possibility that the localization of Nup214 is not just regulated by the FG-rich region, which promotes nuclear accumulation, but that there is another region in Nup214 that could lead to exclusion of the protein from the nuclear volume.

Nup214 is well known to interact with the nuclear export factor CRM1 (Fornerod et al., 1997b; Kehlenbach et al., 1999). Therefore, we investigated the effects of the selective CRM1 inhibitor leptomycin B (LMB; Kudo et al., 1998) on the subcellular localization of transfected Nup214. Strikingly, the localization of full-length Nup214 was shifted from the rim and/or the cytoplasm towards the nucleus upon addition of LMB to the transfected cells (Fig. 2A). This change in localization was irrespective of the nature or the position of the tag (i.e. myc–Nup214, GFP–Nup214, Nup214–GFP, mCherry–Nup214, Nup214–mCherry) (Fig. 2A). We noted, however, that nuclear myc-tagged Nup214 was prone to aggregation, leading to the formation of discrete dots. Furthermore, staining at the nuclear rim was rather weak for Nup214–GFP and myc–Nup214. We therefore used GFP–Nup214 expression constructs for most of our further analyses. Next, we addressed the question of whether the entire population of GFP–Nup214 would shift to the nuclear interior in the presence of LMB, or

whether the protein becomes resistant to the drug upon incorporation into the NPC on its cytoplasmic site. To distinguish between a cytoplasmic and a nuclear localization, we performed differential permeabilization experiments in combination with antibody staining. When the plasma membrane of GFP–Nup214-expressing cells was permeabilized with low concentrations of digitonin, GFP–Nup214 was detected by an anti-GFP antibody, showing that the epitope resides in the cytoplasm, as expected (Fig. 2B). By contrast, a protein of the nuclear lamina, lamin A/C, was not accessible for antibody staining under these conditions. With high concentrations of digitonin, which are known to permeabilize the nuclear membrane as well, lamin A/C was detected, yielding the typical signal at the nuclear rim (Fig. 2B). When cells were incubated with LMB for 2 h, leading to sequestration of GFP–Nup214 in the nucleus, and permeabilized with low concentrations of digitonin, the anti-GFP-antibody still detected GFP–Nup214 at the nuclear rim, but not in the nuclear interior. This result shows that at least part of GFP–Nup214, which is visible as a nuclear rim, remains at the cytoplasmic side of the nuclear envelope, most likely being stably integrated into the NPC. Accordingly, endogenous Nup214 was hardly affected by short treatments of cells with LMB (Fig. 2C), suggesting that proteins that have been inserted into NPCs are resistant to the drug treatment. Extended LMB treatment for 18 h, by contrast, resulted in a partial loss of endogenous Nup214 from the NE and a slight accumulation within the nucleus in many cells (Fig. 2C). For Nup88, this was even more obvious, as the protein accumulated in the nucleus of many such cells, which was not observed in control cells in the absence of LMB. Nup358, by contrast, was not affected by the prolonged treatment of cells with LMB, demonstrating the specificity of the effect. These data suggest that endogenous and overexpressed Nup214 may be recognized as classic, LMB-sensitive CRM1 substrates. Such substrates are characterized by NESs with a specific amino acid composition that mediate their interaction with the export receptor. A search using the LocNES algorithm (Xu et al., 2015) indeed revealed several such potential NES motifs. The NES with the highest score (0.756) was found at position 875–887 of full-length Nup214, with a spacing of hydrophobic (ϕ) and other (x) residues characteristic for a class 1a NES (Kosugi et al., 2008), with an additional hydrophobic residue at the ϕ_0 position (Fig. 2D). The motif is conserved, as it was also found in Nup214 of other vertebrates. A second putative NES with a rather high score (0.665) was found at position 1464–1473. This sequence is conserved in mammals, but not in other vertebrates (data not shown). We next investigated these putative NESs using different approaches.

First, we addressed a possible interaction of the isolated Nup214 NESs, fused to GST, with CRM1. We took advantage of the observation that RanGTP is resistant to RanGAP-induced hydrolysis when it is in a complex with nuclear transport receptors (Bischoff and Görlich, 1997). Because Ran, CRM1 and export cargoes interact with each other in a cooperative manner, RanGAP assays can be used to monitor the formation of trimeric CRM1 export complexes. As shown in Fig. 3A, RanGTP was readily hydrolyzed in the presence of CRM1 and a catalytic amount of RanGAP. The addition of purified snurportin 1 (SPN1), an established cargo protein of CRM1 (Dong et al., 2009; Monecke et al., 2009; Paraskeva et al., 1999), resulted in reduced GTP hydrolysis, indicating the formation of a stable export complex. Likewise, the major part of the first putative Nup214 NES (NES1, corresponding to residues 878–887; note that this peptide lacks the leucine residue at the ϕ_0 position 875) fused to GST clearly reduced hydrolysis on Ran, although slightly higher concentrations than for

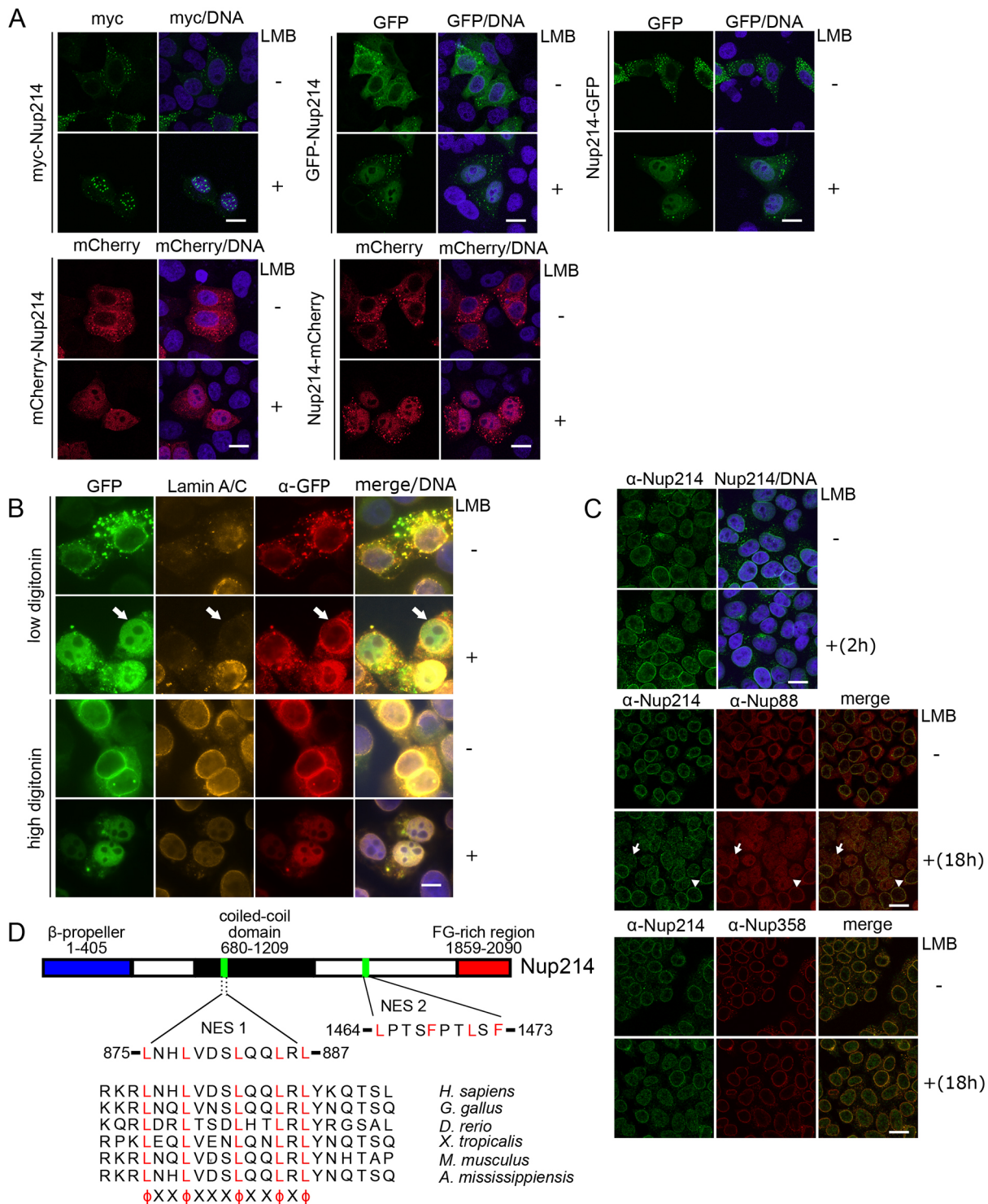


Fig. 2. Nup214 contains a nuclear export sequence. (A) HeLa cells were transfected with plasmids coding for myc-, GFP- and mCherry-tagged versions of Nup214 and treated with or without LMB, as indicated. Proteins were detected by indirect immunofluorescence using anti-myc antibodies or directly via the GFP or mCherry fluorescence. Scale bars: 20 μ m. (B) Differential permeabilization of HeLa cells with low (0.007%) or high (1%) concentrations of digitonin following transfection with a plasmid coding for GFP-Nup214. Cells were either untreated or treated with LMB, as indicated. Proteins were detected directly via GFP fluorescence or by indirect immunofluorescence using anti-GFP (α -GFP) and anti-lamin A/C antibodies. Arrow, cell with a low lamin A/C signal that shows a clear nuclear rim detected by the anti-GFP antibody. Scale bar: 10 μ m. (C) HeLa cells were treated with or without LMB, and proteins were detected by indirect immunofluorescence using anti-Nup214, anti-Nup88 or anti-Nup358 antibodies, as indicated. Arrows, cell with a clear nuclear signal for Nup214 and Nup88. Arrowheads, cell with a clear nuclear rim for both nucleoporins. Scale bars: 20 μ m. In A–C, LMB treatments used 10 nM LMB and were for 2 h unless indicated otherwise. Cells were analyzed by confocal microscopy, and DNA was stained with DAPI (blue). Images are representative of three experiments. (D) Schematic representation of the Nup214 sequence. Two putative NESs are indicated at amino acids 875–887 (NES1, also referred to as NES^{Nup214}) and 1464–1473 (NES2). The sequence of NES1 (875–887) was compared between different vertebrate species (*Homo sapiens*, *Gallus gallus*, *Danio rerio*, *Xenopus tropicalis*, *Mus musculus* and *Alligator mississippiensis*). The hydrophobic residues (ϕ) characteristic for a class 1a NES (Kosugi et al., 2008) are represented in red.

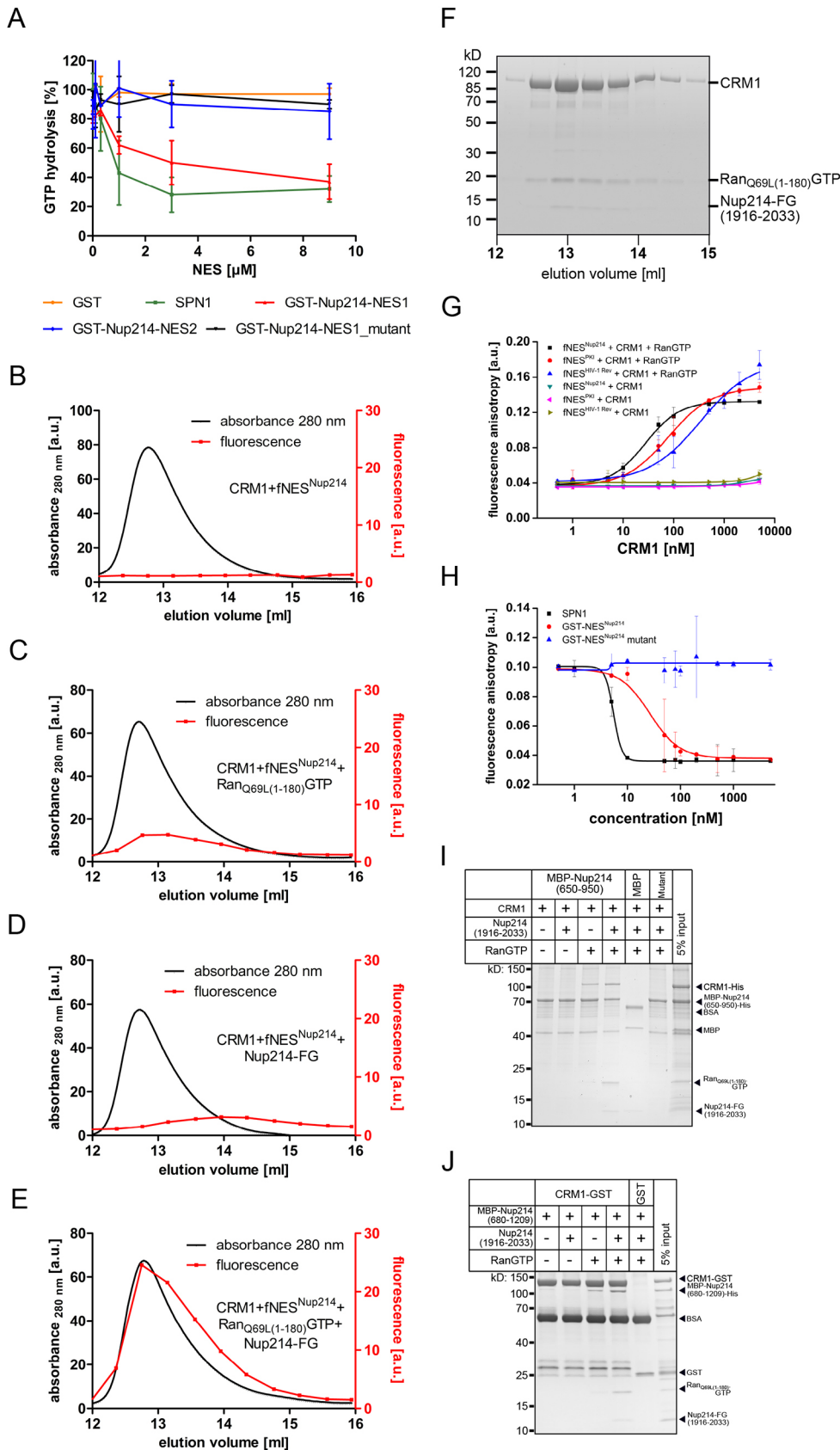


Fig. 3. The Nup214 NES can form a stable export complex with CRM1 in a Ran-dependent manner. (A) RanGAP assays were performed with increasing concentrations of snurportin 1 (SPN1), GST or GST-fusion proteins of the putative NESs as indicated. GST-Nup214-NES1 mutant indicates GST-Nup214 (L878A/L882A/L885A/L887A). Data are presented as the mean \pm s.d. of three independent experiments. (B–E) Complexes of the fluorescent peptide fNES^{Nup214} with (B) CRM1 alone, (C) CRM1 and RanQ69L (1–180)-GTP (RanGTP), (D) CRM1 and an FG-repeat fragment of Nup214 [His–Nup214 (1916–2033), referred to as Nup214-FG], or (E) CRM1, Nup214-FG and RanGTP were analyzed by gel filtration. Absorbance at 280 nm is plotted in black, the fluorescence signal is plotted in red. (F) Fractions from E were analyzed by SDS-PAGE, followed by Coomassie staining. Note that the fluorescent peptide is too small for detection. Data in B–F are representative of four experiments. (G,H) Fluorescence polarization assays. (G) Reactions contained 40 nM of the indicated fluorescent NES peptides and increasing concentrations of CRM1, in the absence or presence of 3 μ M RanGTP, as indicated. Data are presented as the mean \pm s.d. of three independent experiments. (H) Competition assay with fNES^{Nup214} and increasing concentrations of competitors (SPN1 or wild-type or mutant GST-NES^{Nup214}) as indicated. All measurements were performed in the presence of 100 nM CRM1. Error bars show the difference from the mean of two independent experiments. (I,J) CRM1 complexes of Nup214 fragments containing NES^{Nup214}. (I) Wild-type MBP-Nup214 (650–950), MBP-Nup214 650–950 2 \times -mutant or MBP alone were immobilized on amylose beads and incubated in the absence or presence of CRM1, RanGTP and His–Nup214-FG (1916–2033), as indicated. (J) CRM1–GST or GST alone were immobilized on Glutathione Sepharose beads and incubated in the absence or presence of MBP-Nup214 (680–1209), RanGTP and His–Nup214-FG (1916–2033), as indicated. For I and J, bound proteins were analyzed by SDS-PAGE followed by Coomassie staining. Input, 5%. a.u., arbitrary units. Gels shown are representative of two experiments.

SPN1 were required. Neither a mutant version of this NES, where four leucines were exchanged for alanines, nor the second putative NES (NES2, corresponding to residues 1464–1473) nor GST alone

affected GTP hydrolysis, confirming the specificity of the effect and suggesting that amino acids 878–887 (or 875–887, i.e. a sequence including L875 at the ϕ_0 position) of Nup214 might indeed function

as an NES, at least as an isolated peptide. As the putative NES2 did not seem to function as an NES, we focused further investigations on the putative NES1 and renamed it NES^{Nup214}.

In an independent approach, we used fluorescent peptides for the analysis of export complexes. A peptide (fNES^{Nup214}) corresponding to the Nup214 NES including L875 at the ϕ_0 position was chemically synthesized and fluorescently labeled and then used in size exclusion chromatography experiments to monitor complex formation. As shown in Fig. 3B, in the presence of only the peptide, CRM1 eluted from the gel filtration column in a defined peak, with fluorescence remaining at background levels. In the presence of RanGTP, a low level of fNES^{Nup214} could be detected in the peak fractions, indicating the formation of a trimeric complex (Fig. 3C). We have previously shown that such complexes can be further stabilized by an FG-repeat containing fragment of Nup214 (Nup214-FG, corresponding to residues 1916–2033; Port et al., 2015; Roloff et al., 2013). In the presence of such a fragment alone and without RanGTP, fluorescence in the CRM1-containing fractions remained at a low level (Fig. 3D). When all four components (CRM1, fNES^{Nup214}, Nup214-FG and RanGTP) were combined, however, maximum fluorescence levels in the CRM1-containing fraction increased ~4-fold (Fig. 3E). The individual proteins were also detected by SDS-PAGE in the corresponding fractions (Fig. 3F). These results show that export complexes containing fNES^{Nup214} can be formed that are stable enough to resist the conditions of size exclusion chromatography. Next, we used fluorescence polarization to directly measure affinities between different fluorescently labeled NES peptides and CRM1. In this assay, the degree of polarization of the emitted fluorescent light depends on the rotational mobility of the labeled peptide. Hence, changes in polarization, as they occur upon complex formation resulting from the addition of increasing concentrations of CRM1, can be used for the calculation of apparent affinities. We compared the Nup214 NES (fNES^{Nup214}) to the NES of the CRM1 cargo HIV-1 Rev (Fornerod et al., 1997a) and to a modified version of the NES of PKI (heat stable inhibitor of cAMP-dependent protein kinase, also known as PKIA; Güttler et al., 2010; Wen et al., 1995) with respect to export complex formation. As shown in Fig. 3G, of all NESs tested, fNES^{Nup214} had the highest affinity for CRM1 (K_d , 24±6 nM; mean±s.d.). The control peptides exhibited an intermediate (fNES^{PKI}; K_d , 79±5 nM) or low (fNES^{HIV-1 Rev}; K_d , 598±87 nM) affinity. The observed signals were specific for all three peptides, because no changes in polarization were observed in the absence of RanGTP. Finally, we compared the ability of wild-type and mutant GST-NES^{Nup214} to compete with binding of fNES^{Nup214} to CRM1. As a control, we used a high-affinity substrate of CRM1, SPN1. As shown in Fig. 3H, high levels of anisotropy were measured in the absence of a competitor, indicating the presence of export complexes containing fNES^{Nup214}. SPN1 competed with fNES^{Nup214} for CRM1-binding at concentrations below 100 nM. Unlabeled GST-NES^{Nup214} (identical to GST-Nup214-NES1 in Fig. 3A) was also able to compete, although somewhat higher concentrations were needed. The mutant GST-NES^{Nup214}, by contrast, was unable to reduce anisotropy, confirming the specificity of the effects. Taken together, these results show that the Nup214 sequence contains at least one typical NES peptide with a high affinity for the export receptor CRM1.

We next addressed the question of whether this NES can also function in the context of larger Nup214 fragments. First, we immobilized a fusion protein containing the maltose-binding protein (MBP) and a fragment of Nup214 containing the NES

(amino acids 650–950) on beads and investigated its interaction with CRM1. As shown in Fig. 3I, CRM1 alone did not significantly bind to the Nup214 fragment. Upon addition of RanGTP, a clear binding of CRM1 was detected, indicating the formation of an export complex. Binding of CRM1 and Ran was increased when His-Nup214-FG was included in the reaction. No binding of Ran and CRM1 was observed when MBP alone or a mutant version of MBP-Nup214 [Nup214 650–950 (L878A/L882A), also referred to as Nup214 650–950 2×-mutant] had been immobilized on beads. In a complementary experiment, we immobilized CRM1-GST on beads and analyzed binding of a Nup214 fragment containing the NES [MBP-Nup214 (680–1209)], again in the absence or presence of RanGTP or Nup214-FG (Fig. 3J). Similar to the results described above, binding of MBP-Nup214 (680–1209) was only observed in the presence of Ran. Furthermore, binding of MBP-Nup214 (680–1209) and of Ran was enhanced in the presence of Nup214-FG. No binding was detected when GST instead of GST-CRM1 had been immobilized, confirming the specificity of the interactions. Taken together, our biochemical analyses showed that Nup214 contains at least one sequence that mediates RanGTP-dependent binding to CRM1, as demonstrated at the level of an isolated peptide and in the context of larger Nup214 fragments.

The Nup214 NES is functional in nuclear export

To address the functionality of the putative NESs, we investigated the subcellular localization of Nup214 fragments. First, GFP-tagged isolated Nup214 NES (GFP-NES^{Nup214}) was transfected. GFP-NES^{Nup214} was clearly excluded from the nucleus (Fig. 4A). As a control, two or four of the NES-defining hydrophobic residues were mutated, yielding GFP-NES^{Nup214} 2×-mutant (corresponding to mutations L878A and L882A) or GFP-NES^{Nup214} 4×-mutant (corresponding to mutations L878A, L882A, L885A and L887A), respectively. Both NES mutants clearly localized to the nucleus, confirming the importance of the NES-defining residues for nuclear export. The second putative NES (amino acids 1464–1473) was analyzed in the same way. Both fusion proteins [wild-type and an L1464A/F1468A double mutant; this mutation is marked with an asterisk (*) in all following constructs] showed a similar nuclear localization, with very low levels of fluorescence observed in the cytoplasm (Fig. 4A). Taken together, these results confirm the biochemical analyses (Fig. 3), showing that NES^{Nup214} is active and able to export GFP out of the nucleus. The second NES sequence, by contrast, shows no or only very weak activity *in vivo*, at least as an isolated peptide.

Next, we analyzed the effect of a double-mutation (L878A/L882A; 2×-mutant) on a larger fragment of Nup214 containing NES^{Nup214}, GFP-Nup214 (680–1209). As shown in Fig. 4B, the wild-type form of the fragment was found in the cytoplasm (compare with Fig. 1B) and accumulated in the nucleus in the presence of LMB. Likewise, the mutant version of the fragment was found in the nucleus.

Finally, we incorporated the same Nup214 NES mutations in full-length GFP-Nup214, yielding GFP-Nup214 2×-mutant (i.e. L878A/L882A) and GFP-Nup214 4×-mutant (i.e. L878A/L882A/L885A/L887A) and analyzed the subcellular localization of the proteins in a quantitative manner (Fig. 4C,D). As seen before, wild-type GFP-Nup214 was found at the nuclear rim and also in the cytoplasm, with only 11% of cells having a nuclear:cytoplasmic signal ratio greater than one. Exchanging two (L878A/L882A) or four (L878A/L882A/L885A/L887A) leucine residues in the NES with alanines increased this level to 39% or 71%, respectively. We then addressed the question of whether the second putative NES,

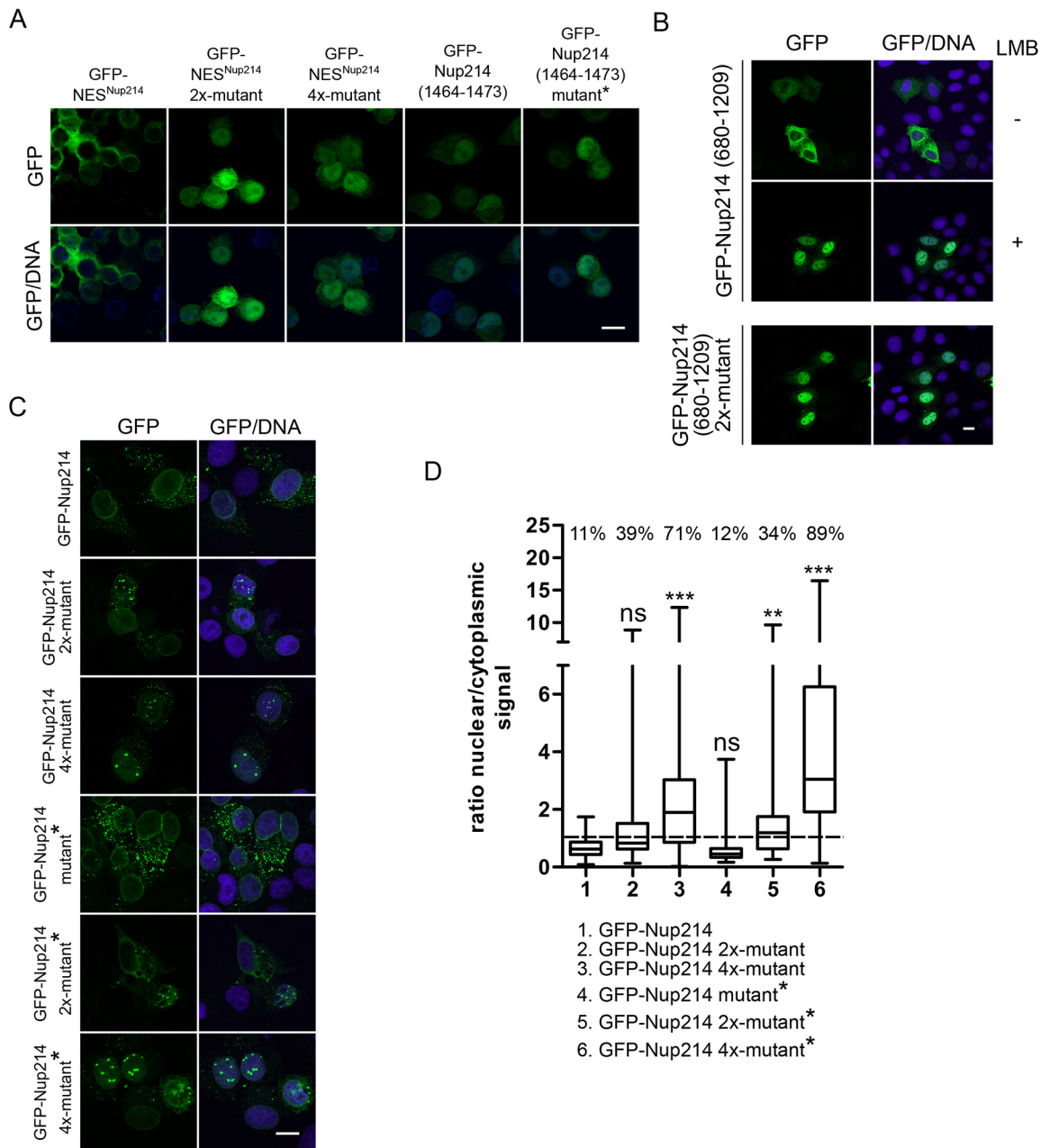


Fig. 4. Mutations in NES^{Nup214} inhibit export of Nup214. (A) HeLa cells were transfected with expression constructs encoding wild-type and mutant versions of GFP-NES^{Nup214} as indicated. (B) HeLa cells were transfected with plasmids encoding the wild-type or the 2x-mutant version of GFP-Nup214 (680–1209). Where indicated, cells were treated with 10 nM LMB for 2 h. Images in A,B are representative of three experiments. (C,D) HeLa cells were transfected with plasmids encoding wild-type or mutant versions of full-length GFP-tagged Nup214 as indicated. (D) Quantitative analysis of the subcellular localization of the GFP-fusion proteins shown in C. The mean fluorescence intensities were measured in the nucleus and the cytoplasm of cells ($n=20-30$) from at least four independent experiments (i.e. a total of 80–120 cells) and the ratios of nuclear:cytoplasmic signal intensity were plotted. Boxes represent the 25th to 75th percentiles, the lines within the boxes represent the median and the whiskers represent the minimum and maximum values. A minimum threshold ratio of one is indicated by a dashed line, and the number of cells above the threshold are indicated as the percentage of the total number of cells. *** $P<0.001$; ** $P<0.01$; ns, not significant (with respect to condition 1; one-way ANOVA with Dunnett's post hoc test). In A–C, DNA was stained with DAPI (blue) and cells were analyzed by confocal microscopy. Scale bars: 20 μ m.

which on its own did not interact with CRM1 *in vitro* (Fig. 3A) and was not active *in vivo* (Fig. 4A), could exert an effect in the context of the full-length protein. GFP-Nup214 mutant* (i.e. L1464A/F1468A) localized to the nuclear rim and the cytoplasm, very similar to the wild-type protein. Combining mutations in the two putative NESs failed to enhance the nuclear localization of one resulting fusion protein (GFP-Nup214 2x-mutant*) but resulted in a slight increase in the nuclear localization of another (GFP-

Nup214 4x-mutant*); with 89% of cells expressing the mutant form showing a nuclear:cytoplasmic signal ratio greater than one, compared to 71% of cells expressing the GFP-Nup214 4x-mutant form).

Taken together, our biochemical and cell biological analyses show that Nup214 contains at least one classic NES (amino acids 878–887), allowing CRM1-dependent export of the nucleoporin from the nucleus to the cytoplasm.

Nuclear Nup214 sequesters soluble nuclear export factors and nucleoporins

Some tagged versions of Nup214 had the tendency to form dot-like structures, either in the cytoplasm or in the nucleus (Fig. 1A). These structures are reminiscent of dots as observed for Nup214 fusion proteins that are known from certain chromosomal rearrangements in leukemia (Fornerod et al., 1995; Port et al., 2016; Saito et al., 2004) and that were described to sequester certain transport factors, including several nucleoporins (Oka et al., 2016; Port et al., 2016). First, we used the aliphatic alcohol 1,6-hexanediol to distinguish between liquid-like assemblies and solid-like aggregates (Kroschwald et al., 2017; Ribbeck and Görlich, 2002). As shown in Fig. S1, treatment of cells that had been transfected with GFP–Nup214 (i.e. the wild-type version of the nucleoporin) with 1,6-hexanediol had no effect on the cytoplasmic aggregates often seen with this fusion protein. Nuclear dots, as observed with the GFP–Nup214 4×-mutant*, by contrast, were partially dissolved by the alcohol. Next, we analyzed the GFP–Nup214 dots for a possible colocalization with endogenous nuclear transport factors, as described previously for the fusion proteins Set–Nup214, Dek–Nup214 and SQSTM1–Nup214 (Fornerod et al., 1995; Port et al., 2016). As shown in Fig. 5A, the soluble factors CRM1 and Ran both showed a partial colocalization with wild-type GFP–Nup214 in dots that were formed in the cytoplasm of overexpressing cells. Similarly, CRM1 and Ran were found in nuclear dots, together with the NES mutant GFP–Nup214 4×-mutant. Next, we addressed the localization of nucleoporins in cells expressing the wild-type GFP–Nup214 or GFP–Nup214 4×-mutant. As shown in Fig. 5B, three nucleoporins (Nup62, Nup88 and Nup98) were found in cytoplasmic dots with wild-type GFP–Nup214. Nup88 and Nup62, but not Nup98, were also found in the nuclear dots of cells expressing GFP–Nup214 4×-mutant. Three other nucleoporins, Nup358, Nup153 and ELYS, were not affected by wild-type or mutant GFP–Nup214. The occurrence of nuclear dots containing a specific set of nucleoporins and of soluble transport factors is thus a common phenotype of cells expressing the oncogenic fusion proteins of Nup214 (Mendes and Fahrenkrog, 2019) or the NES mutant of Nup214. We finally treated cells overexpressing myc–Nup214 with LMB (compare with Fig. 2A) and analyzed transfected cells with respect to the localization of endogenous Nup88. As seen for the mutant Nup214 (Fig. 5B), nuclear myc–Nup214 also recruited Nup88 to dot-like structures (Fig. 5C). Similarly, endogenous Nup88 colocalized with a mutant version of myc–Nup214 (L878A/L882A, also referred to as myc–Nup214 2×-mutant) in nuclear dots, also in the absence of LMB.

An artificial NES can substitute for the endogenous NES of Nup214

It has previously been shown that full-length Nup214 can enter the nucleus under certain conditions (Boer et al., 1998). Here, we have shown that it contains at least one bona fide NES that allows its re-export to the cytoplasmic side of the NPC by CRM1. We next tested whether an artificial NES at a different location could substitute for the endogenous NES within the coiled-coil region of the protein. First, we used only a small fragment of the nucleoporin [GFP–Nup214 (1969–2090)] to address the functionality of the Nup214 NES (NES^{Nup214}) in the context of the FG repeats. In contrast to the nuclear localization of GFP–Nup214 (1969–2090) alone (compare with Fig. 1B), GFP–Nup214 (1969–2090)-NES^{Nup214} largely localized to the cytoplasm (Fig. 6A). Addition of LMB resulted in a clear nuclear accumulation of the fusion protein, demonstrating the functionality of the NES (Fig. 6A). Next, we used the mutant

versions of full-length Nup214 (GFP–Nup214 4×-mutant and GFP–Nup214 4×-mutant*) and linked the NES^{Nup214} or the HIV-1 Rev NES (Fischer et al., 1995), NES^{HIV-1 Rev}, to their C-terminal ends. Both NESs were able to export the GFP-tagged protein out of the nucleus, as essentially all transfected cells showed a cytoplasmic localization of the respective proteins, in contrast to the nucleoporin lacking a C-terminal NES (Fig. 6B). Furthermore, many cells exhibited a nuclear rim, in particular cells expressing the mutant versions of GFP–Nup214 with NES^{Nup214} at the C-terminus. Addition of LMB to transfected cells resulted in a nuclear localization of the fusion proteins, again confirming the functionality of the NESs. Taken together, our results show that an internal NES or an artificial NES at the very C-terminus of Nup214 promotes its transport to the cytoplasmic side of the NE and, possibly, incorporation into the NPC.

Interaction of Nup214 with Nup88

The identified Nup214 NES is located in the putative coiled-coil region of the nucleoporin, which is expected to interact with Nup88 (Fornerod et al., 1996). Because hydrophobic residues, as they occur in classic NESs, are also characteristic of the heptad repeats of coiled-coil regions, we investigated the interaction of wild-type and mutant Nup214 with endogenous Nup88 in more detail. First, we performed co-immunoprecipitation experiments to biochemically confirm the interaction of Nup88 with Nup214. Cells were transfected with plasmids encoding wild-type, 2×-mutant- or 4×-mutant versions of GFP–Nup214 (680–1209). Wild-type and mutant GFP–Nup214 (680–1209), but not GFP alone were able to co-precipitate endogenous Nup88 (Fig. 7A). Second, we transfected cells with full-length versions of GFP–Nup214 (wild-type, 4×-mutant, 4×-mutant–NES^{Nup214}, 4×-mutant* and 4×-mutant*–NES^{Nup214}; Fig. 7B). Again, endogenous Nup88 could be co-precipitated with all versions. Together, these results clearly demonstrate that the mutant versions of Nup214, where the NES at position 875–887 is inactivated by leucine to alanine mutations, are still able to interact with Nup88.

Next, we investigated whether exogenous Nup214 could also target endogenous Nup88 to the nuclear pore in cells where endogenous Nup214 had been depleted by specific siRNAs. The efficiency of the depletion was assessed using immunoblotting (Fig. 7C). As shown in Fig. 7D, the downregulation of endogenous Nup214 resulted in a loss of Nup88 from the nuclear pore, as described previously (Bernad et al., 2004; Hutten and Kehlenbach, 2006). Strikingly, the expression of either GFP–Nup214 or of the NES mutant version containing the C-terminal NES (GFP–Nup214 4×-mutant–NES^{Nup214}) from siRNA-resistant plasmids resulted in a clear nuclear rim for Nup88 in GFP-positive cells (Fig. 7D). The mutant lacking the C-terminal NES, by contrast, failed to localize Nup88 to the nuclear rim, leading to intranuclear dots instead. This result clearly shows that the folding of the Nup214 mutant is not compromised, as it correctly directs its physiological binding partner, Nup88, to the NPC, probably leading to correct incorporation of both proteins into the complex. Furthermore, it suggests that residues in the coiled-coil domain other than the NES motif mediate Nup214–Nup88 interaction.

GFP–NUP214 is integrated into the NPC

Potentially, the nuclear rim localization as observed for the GFP–Nup214 fusion proteins under different conditions could result from two different binding modes of Nup214. First, Nup214 could be part of a rather transient transport complex, where GFP–Nup214 associates as a high-affinity export cargo with CRM1, RanGTP and,

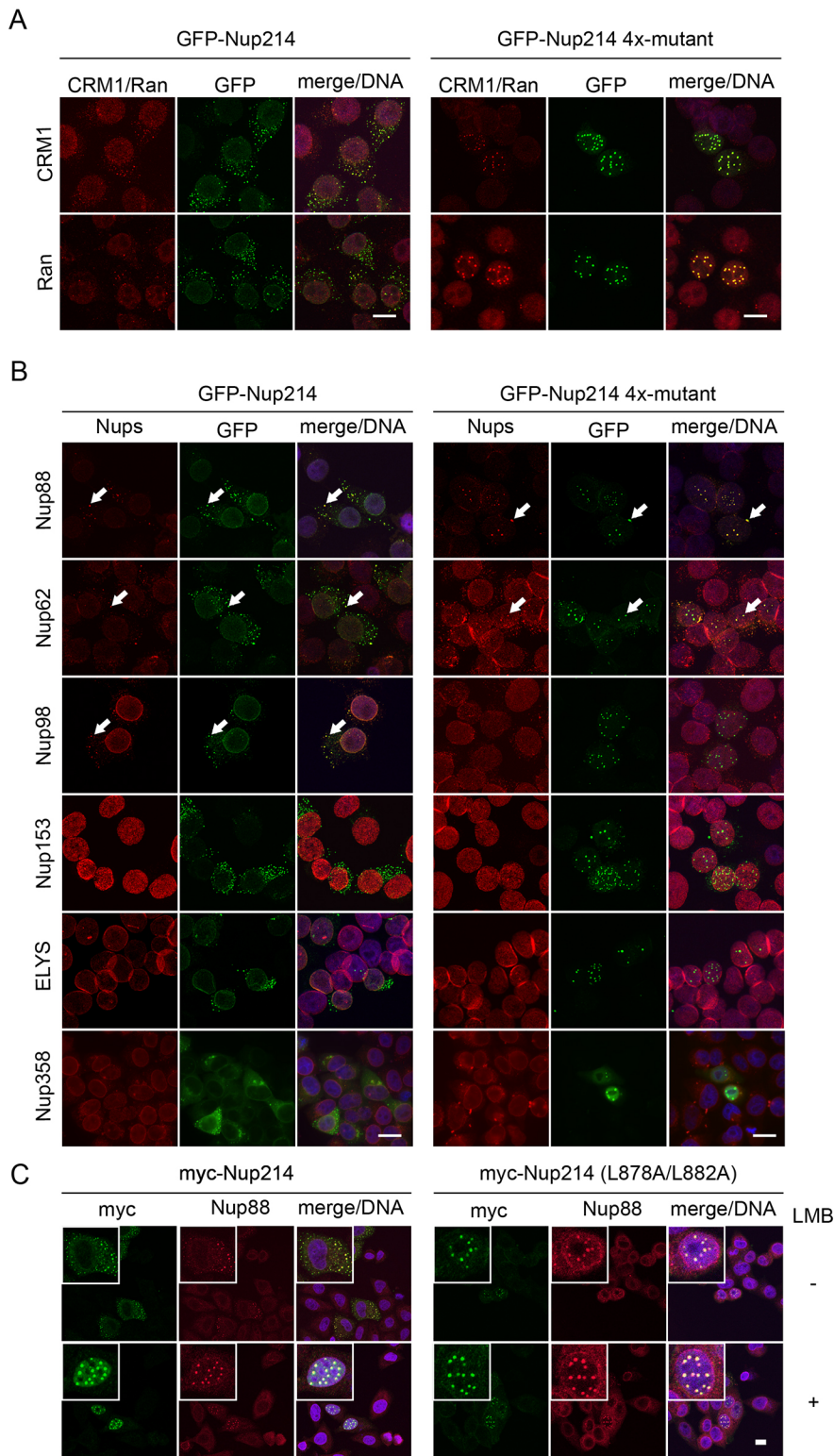


Fig. 5. Nup214 recruits transport factors and nucleoporins. (A) HeLa cells were transfected with expression constructs encoding the wild-type or the 4x-mutant version of full-length GFP-Nup214 as indicated. Cells were analyzed by indirect immunofluorescence using anti-CRM1 and anti-Ran antibodies. (B) HeLa cells were transfected as in A, and indirect immunofluorescence was used to detect endogenous nucleoporins, as indicated. Arrows point to colocalizing proteins. (C) HeLa cells were transfected with expression constructs encoding the wild-type or a mutant version (L878A/L882A) of full-length myc-Nup214 and treated with LMB for 2 h, as indicated. Cells were analyzed by indirect immunofluorescence using anti-Nup88 and anti-myc antibodies. Insets show magnifications of a single cell expressing myc-Nup214. In A–C, DNA was stained with DAPI (blue). Confocal microscopy was used for the analyses, except for Nup358 samples in Fig. 5B, where a widefield fluorescence microscope was used. Images are representative of two experiments. Scale bars: 20 μ m (A,B), 10 μ m (C).

for example, Nup358. Indeed, Nup358-dependent binding of CRM1 to the NE has been shown previously (Engelsma et al., 2004; Hutten and Kehlenbach, 2006). Furthermore, RanGTP and an export cargo have been shown to enhance the affinity of CRM1 for Nup358 (Ritterhoff et al., 2016). Second, the rim localization could result from a more stable complex, where full-length GFP-Nup214 is an integral component of the NPC (i.e. a bona fide nucleoporin). To distinguish between these possibilities, we performed

experiments in digitonin-permeabilized cells. An export complex, even with a cargo containing a high-affinity NES, is expected to disassemble in the presence of RanBP1 and RanGAP. We therefore permeabilized cells expressing either full-length GFP-Nup214 (wild-type or GFP-Nup214 4x-mutant*-NES^{Nup214}) with digitonin. As shown in Fig. 8, the GFP-tagged proteins were largely observed at the level of the nuclear envelope, with little signal in the cytoplasmic region. Intact cells, by contrast, showed a

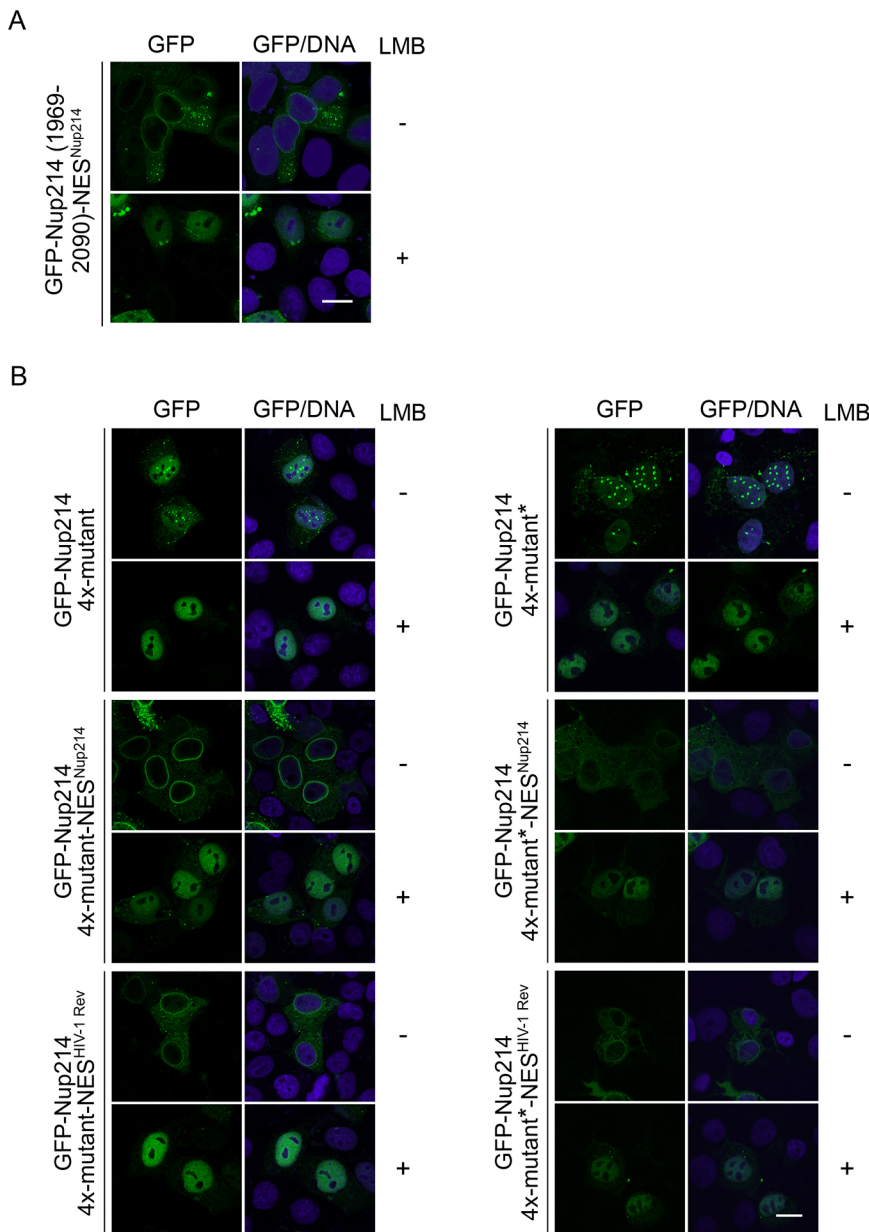


Fig. 6. NES sequences inserted at the C-terminus promote nuclear export of Nup214 with mutations in the NES. (A) HeLa cells were transfected with a plasmid encoding GFP–Nup214 (1969–2090)-NES^{Nup214}. (B) HeLa cells were transfected with plasmids encoding mutant full-length GFP–Nup214 4×-mutant or GFP–Nup214 4×-mutant* lacking a C-terminal NES sequence (top) or containing a C-terminal NES sequence derived from Nup214 (middle) or the HIV-1 Rev protein (bottom), as indicated. In A and B, cells were treated with or without 10 nM LMB for 2 h, as indicated. DNA was stained with DAPI (blue) and cells were analyzed by confocal microscopy. Images are representative of three experiments. Scale bars: 20 μm.

certain level of cytoplasmic signal (compare Fig. 1B, Fig. 2A and Fig. 6B). When cells were incubated with RanBP1 and/or RanGAP, the GFP fluorescence at the nuclear envelope remained at a high level, demonstrating that the full-length versions of GFP–Nup214 were not released from the NE under our experimental conditions. These results suggest that the fusion proteins are stably incorporated into the NPC as bona fide nucleoporins.

DISCUSSION

Nup214 contains an NES and is exported from the nucleus in a CRM1-dependent manner

Nup214 is an established interaction partner of CRM1 (Fornerod et al., 1997b; Kehlenbach et al., 1999), which functions in nuclear protein export of subset of CRM1 cargoes (Bernad et al., 2006; Hutten and Kehlenbach, 2006). So far, structural and functional analyses of CRM1–Nup214 complexes have focused on the FG repeats of Nup214. It therefore came as a surprise that Nup214 can also interact with CRM1 in a transport cargo-specific mode via a classic NES at position 875–887. Using bioinformatic tools, such

sequences can be identified in a large number of proteins. However, only a subset of these putative motifs has been validated as functional NESs in the context of full-length proteins. With their characteristic hydrophobic residues, putative NESs might be buried in the hydrophobic core of folded proteins and, thus, not be accessible for the soluble export factor CRM1. A prominent example of this is the tyrosine kinase Bcr–Abl (Hantschel et al., 2005). For Nup214, this is probably not the case, because both the isolated NES peptide (Fig. 3A–H) and also longer fragments of Nup214 containing the NES (Fig. 3I,J) interact with CRM1 in a Ran-dependent manner. Furthermore, full-length Nup214 was affected by LMB when overexpressed in cells, and mutations in the NES of Nup214 fragments and full-length proteins resulted in their nuclear accumulation. The observations that (1) endogenous Nup88 can interact with all tested mutants (Fig. 5B and Fig. 7B) and (2) a mutant Nup214 protein with a C-terminal NES (GFP–Nup214 4×-mutant NES^{Nup214}) leads to incorporation of Nup88 into the NPC in cells where endogenous Nup214 is depleted (Fig. 7D) suggest that the overall structure of the mutants is not compromised.

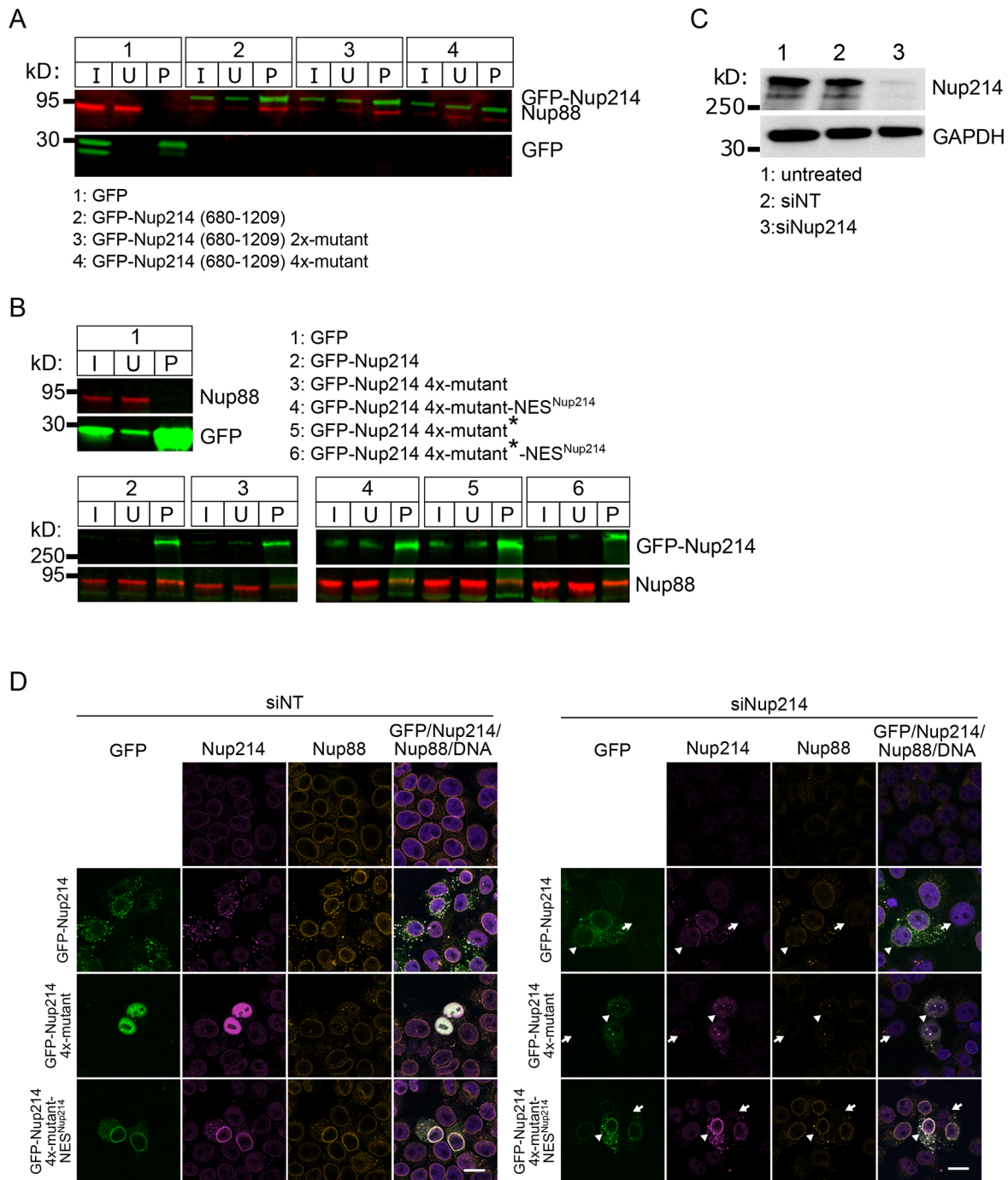


Fig. 7. The Nup214 NES promotes targeting of Nup88 to the NPC. (A) HEK 293T cells were transfected with plasmids encoding wild-type (2) or mutant (3,4) GFP-Nup214 (680–1209) fragments. GFP (1) was used as a control. (B) HEK 293T cells were transfected with plasmids encoding full-length wild-type (2) or mutant (3–6) GFP-Nup214, as indicated. GFP (1) was used as a control. In A and B, cells were lysed, and immunoprecipitation was performed using GFP-trap. Proteins in input lysates (5%, I), unbound (U) and immunoprecipitated samples (P) were analyzed by SDS-PAGE and immunoblotting using anti-GFP (green) and anti-Nup88 (red) antibodies. Blots shown are representative of three experiments. (C) HeLa cells were treated with siRNAs against Nup214 (siNup214) or non-targeting control siRNAs (siNT). Total cell lysates were subjected to SDS-PAGE, followed by immunoblotting to detect Nup214. GAPDH was used as a loading control. Blot is representative of three experiments. (D) HeLa cells were treated with siRNAs against Nup214 (siNup214) or non-targeting control siRNAs (siNT) and transfected with plasmids encoding wild-type full-length GFP-Nup214 or mutant versions of GFP-Nup214 containing or lacking a C-terminal NES, as indicated. Top row shows cells that were treated with siNT or siNup214. Cells were subjected to indirect immunofluorescence using antibodies against Nup214 and Nup88 and analyzed by confocal microscopy. DNA was stained with DAPI (blue). Arrowheads, GFP-Nup214-expressing cells; arrows, Nup214-depleted cells without GFP-Nup214 signal. Images are representative of three experiments. Scale bars: 20 μ m.

Stable incorporation of the mutant GFP-Nup214 itself is also supported by the results shown in Fig. 8. Interestingly, endogenous Nup214 was not affected by short treatments with LMB (Fig. 2C),

suggesting that upon insertion into the NPC, the protein is not subject to constant shuttling, as expected for a bona fide nucleoporin. After 18 h of LMB treatment, by contrast, Nup214

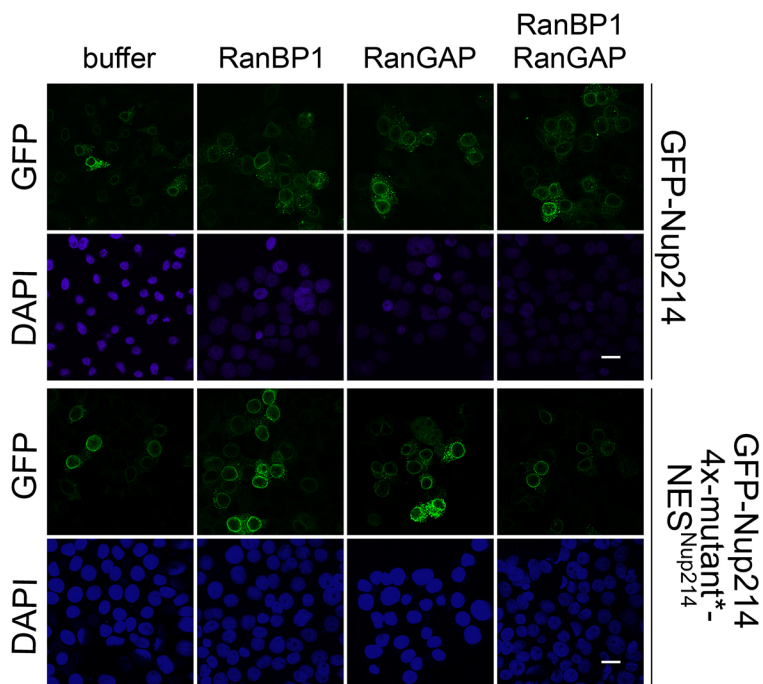


Fig. 8. Wild-type and mutant versions of full-length GFP–Nup214 are stably inserted into the NPC. HeLa cells were transfected with plasmids encoding GFP–Nup214 or GFP–Nup214 4x-mutant*–NES^{Nup214} as indicated. Cells were permeabilized with 0.007% digitonin, incubated with either buffer, 500 nM RanBP1 and/or 500 nM RanGAP at room temperature for 30 min, as indicated, and analyzed by confocal microscopy. DNA was stained with DAPI. Note that permeabilization is expected to lead to a partial loss of initially cytoplasmic proteins, including under control conditions (buffer). Images are representative of three experiments. Scale bars: 20 μ m.

was partially lost from the nuclear envelope and, together with Nup88, accumulated in the nucleus. It remains to be investigated whether this reflects a very slow release from its binding site at the NPC and/or a defect in the incorporation of newly synthesized Nup214 into the pore. Interestingly, only a subset of cells showed an accumulation of Nup214 and Nup88. This might reflect the different mechanisms that lead to the formation of novel NPCs during interphase and after mitosis.

The identified NES in Nup214 corresponds to a characteristic class 1a NES (Kosugi et al., 2008). It also has a hydrophobic residue at the ϕ_0 -position, suggesting a high affinity for CRM1 (Güttler et al., 2010). Indeed, our fluorescence polarization assays pointed to a rather tight interaction between CRM1 and the Nup214 NES, compared to that of other NESs of described CRM1 cargoes. In binding assays using the isolated peptide (Fig. 3E) or larger Nup214 fragments containing the NES (Fig. 3I,J), binding was further increased by an FG repeat-containing fragment of Nup214 (1916–2033), similar to our previous observations (Hutten and Kehlenbach, 2006; Port et al., 2015; Roloff et al., 2013). Such a fragment was shown to stabilize trimeric export complexes containing CRM1, RanGTP and an export cargo, with contacts to N- and C-terminal regions of CRM1 (Port et al., 2015; Roloff et al., 2013). It remains to be investigated whether a single Nup214 molecule can interact with CRM1 via its NES and the FG-rich region at its C-terminus at the same time.

In contrast to NES1 (amino acids 875–887; NES^{Nup214}), the sequence with the second highest score (NES2, amino acids 1464–1473) could not be confirmed as an NES. In isolation, it was not functional (Fig. 3A, Fig. 4A), and in the context of full-length Nup214, mutations had no or very minor effects (Fig. 4C,D).

What are the consequences of Nup214 residing in the nucleus, either resulting from mutations in the protein sequence or from treatment of cells with LMB? Our observations are similar to those made for oncogenic fusion proteins of Nup214, which accumulate in the nucleus and lead to the recruitment of physiological direct or indirect binding partners of the nucleoporin (Formerod et al., 1995; Port et al., 2016; for a review see Mendes and Fahrenkrog, 2019).

These include Ran and CRM1 (Fig. 5A) and the nucleoporins Nup62 and Nup88 (Fig. 5B). In overexpressing cells, not only nuclear, but also cytoplasmic dots containing wild-type GFP–Nup214 or Nup214–mCherry were observed (Fig. 2A). These cytoplasmic structures, which also recruited endogenous Nup62, Nup88 and Nup98 (Fig. 5B), were not dissolved by hexanediol (Fig. S1), suggesting that they are aggregates resulting from overexpression of the nucleoporin. Nup214 contains intrinsically disordered regions, which tend to undergo a phase transition leading to the formation of liquid droplets (Brangwynne, 2013). Such nuclear droplets can be highly dynamic (Port et al., 2016) and can dissolve in the presence of hexanediol (Fig. S1) and LMB (Fig. 6B). They may serve as binding platforms for the physiological interaction partners of the seed, in our case overexpressed Nup214. The observation that nuclear aggregates containing Nup214 fusion proteins dissolve upon the addition of LMB has been made previously (Port et al., 2016; Saito et al., 2016). It points to a scaffolding effect of Nup214 that recruits other nucleoporins, Ran, CRM1 and export cargoes. In the presence of LMB, the interaction of CRM1 with all its cargoes is reduced, leading to a more homogenous distribution of all components, including the Nup214 fusion protein.

Possible physiological functions of the Nup214 NES

The NPC is a remarkably symmetric complex with a striking rotational eight-fold symmetry. With respect to the plane of the nuclear envelope, symmetric and asymmetric nucleoporins have been identified. The symmetric proteins of the Y-complex, for example, occur in copy numbers of 32 (Ori et al., 2013) in outer nuclear and cytoplasmic rings (Ashkenazy-Titelman et al., 2020). Nup153 and Tpr, on the other hand, are asymmetric, as they are present only on the nuclear side of the NPC. Likewise, a few nucleoporins, including Nup358 and Nup214, are found only on its cytoplasmic side. This raises the important question of how this asymmetry is established during the biogenesis of the NPC and then maintained. This has been very elegantly shown for Nup153, when novel NPCs are formed during interphase. Nup153 contains a nuclear localization signal (NLS) and interacts with the nuclear

transport receptor transportin (Nakielny et al., 1999). In the cytoplasm, transportin prevents binding of Nup153 to the outer nuclear membrane (and to other membranes as well). After import, RanGTP dissociates the transportin–Nup153 complex, and the nucleoporin can interact specifically with the inner nuclear membrane via an N-terminal amphipathic helix (Vollmer et al., 2015). In the next step, Nup153 then recruits the Y-complex to the inner nuclear membrane, thus initiating the formation of a novel pore complex. The second asymmetric nuclear nucleoporin, Tpr, can also be actively imported into the nucleus, namely via the importin α/β pathway (Ben-Efraim et al., 2009; Snow et al., 2013). Hence, fast and efficient nuclear import seems to be a major mechanism to prevent incorporation of asymmetric nucleoporins from the wrong side of the nuclear envelope, at least during interphase. For the major cytoplasmic nucleoporins, correct incorporation appears straightforward at first sight: Nup214 and Nup358 are very large proteins, which, upon synthesis, should not accumulate on the wrong (i.e. the nuclear) side of the nuclear envelope. Nup214 in particular, however, is very rich in FG repeats, which can act as transport receptor-independent NLSs, explaining the accumulation of FG fragments in the nucleus (Formerod et al., 1996). Furthermore, transport receptors interact with FG repeats and may lead to co-import of Nup214 by a piggyback mechanism. Hence, newly synthesized Nup214 faces a certain chance of ending up in the nucleus during interphase, prior to proper and side-specific incorporation into either a nascent NPC or an NPC that undergoes structural rearrangements (e.g. the exchange of old against new nucleoporins). Our identification of an active NES in Nup214 now provides a simple explanation for the observed asymmetry of the protein. Nup214 that reaches the nuclear interior by one or the other mechanism can be exported back to the cytoplasm by the classic nuclear export receptor CRM1. Such a mechanism would prevent the incorporation of Nup214 into the NPC from its nuclear side during interphase. A similar mechanism might be at play in postmitotic NPC assembly, where Nup214 is one of the last nucleoporins that associates with novel pores, probably at a point where transport competence has already been established (Dultz et al., 2008). Nup214 that was trapped inside the nucleus prior to formation of a novel nuclear envelope could thus be exported to the cytoplasm and then be inserted into novel pores from the correct side. An inefficient retrieval system could thus lead to insertion from the nuclear (i.e. the ‘wrong’) side. Indeed, small amounts of endogenous and overexpressed Nup214 have been detected on the nuclear side of the NPC using immunoelectron microscopy (Paulillo et al., 2005, 2006). It is unclear exactly how Nup214 or the Nup214 complex is linked to the rest of the pore. Biochemically, an interaction between Nup214 and Nup188 has been demonstrated (von Appen et al., 2015). Nup188 is a component of the Nup93 complex (also called the inner ring complex) and may well present a potential binding site for Nup214 also on the nuclear side of the NPC.

NES-dependent incorporation of Nup214 into the NPC may also be promoted by an export-independent mechanism. Upon synthesis, soluble Nup214 could interact with CRM1 in the cytoplasm in the vicinity of the NPC, where Ran in its GTP-bound form should be present at a certain concentration (i.e. prior to GTP hydrolysis as induced by cytoplasmic RanGAP). Such a Nup214–CRM1 complex could then interact with Nup358 at the cytoplasmic side of the NPC. This giant nucleoporin was previously suggested to serve as a binding platform for CRM1-containing export complexes (Ritterhoff et al., 2016). Upon GTP hydrolysis, promoted by Nup358-associated RanGAP, Nup214 would then be free for stable

insertion into the NPC. Such a role of Nup358 as a binding platform can also be envisaged in the export-dependent mechanism as described above. Interestingly, Nup358-dependent localization of Nup214 to the NPC has been suggested (Bernad et al., 2004), although this was not observed in another study (Hutten and Kehlenbach, 2006). We are currently testing these ideas of Nup214 NES functions in the biogenesis of the NPC. One important question concerns the exact timing of the formation of NPC subcomplexes (e.g. the Nup214–Nup88–Nup62 complex). Previous work has suggested that Nup88 and Nup214 associate prior to their stable integration into the NPC (Bastos et al., 1997). Similar results were reported recently for the yeast homologs Nup82 and Nup159 (Onischenko et al., 2020). It is unclear, however, if all components of such subcomplexes are synthesized in stoichiometric amounts, leading to complex formation immediately after translation, or if free nucleoporins occur as well.

Besides a possible role in NPC biogenesis, the Nup214 NES may function in CRM1-dependent nuclear export. It is generally assumed that export complexes disassemble when they reach the cytoplasmic side of the NPC, resulting from RanGAP-promoted hydrolysis on RanGTP. A substantial portion of cellular RanGAP in fact associates with the NPC, as it is stably bound to Nup358 (Mahajan et al., 1997; Matunis et al., 1996). As described above, CRM1-containing export complexes may interact with Nup358 on the cytoplasmic side of the NPC (Ritterhoff et al., 2016). Because Nup214 is found in close proximity to Nup358, the Nup214 NES may support the dissociation of such complexes, simply by competition with the NES of certain soluble export cargoes. Accordingly, Nup214 has been shown in siRNA-depletion experiments to be required for nuclear export of a subset of cargoes (Bernad et al., 2006; Hutten and Kehlenbach, 2006; Kindermann et al., 2019). It remains an open question why other cargoes are insensitive to changes in cellular Nup214 levels. Interestingly, a similar mode of action was suggested for an NLS-like sequence in Nup98 during disassembly of import complexes on the nuclear side of the NPC (Fontoura et al., 2000).

Taken together, the findings of this study add Nup214 to the short list of nucleoporins that undergo NTR-dependent nuclear transport. Interestingly, a putative NES was recently identified in one of the binding partners of Nup214, Nup62 (Baumhardt et al., 2020). The functionality and the significance of this sequence, however, were not investigated.

MATERIALS AND METHODS

Cloning

His–Nup214 (1916–2033)–His (Port et al., 2015), pET21a–His–CRM1–His (obtained from Dr Ralf Ficner, Institute of Microbiology and Genetics, Göttingen, Germany; Shaikhqasem et al., 2020) and His₁₀ZZ–[TEV]–RanQ69L_{1–180} (Monecke et al., 2009; obtained from Dr Dirk Görlich, Max Planck Institute for Biophysical Chemistry, Göttingen, Germany) were described previously. A plasmid containing the coding sequence for human Nup214 was originally obtained from Dr Gerard Grosveld (Jude Children’s Research Hospital, Memphis, TN, USA). For generation of other plasmids see Table S1. Site-direct mutagenesis was performed using the parent vector and sense and antisense oligonucleotides containing the mutation sites (as indicated in Table S1). The annealing temperature was set at 60°C for all primer pairs and the elongation time was chosen based on the expected PCR product size (30 s/kb). DpnI (10 U, Thermo Fisher Scientific) was added for 1–2 h at 37°C to the reactions to degrade the templates. PCR products were transformed in *E. coli* DH5 α using a standard protocol.

Protein expression and purification

Expression and purification of snurportin 1 (Strasser et al., 2004), GST–CRM1 (Strasser et al., 2004), CRM1–His (Shaikhqasem et al., 2020),

RanQ69L (amino acids 1–180) (Port et al., 2015), RanBP1 (Port et al., 2015) and RanGAP (Mahajan et al., 1997), as well as GTP loading of Ran (Kehlenbach et al., 1998) was performed according to previously published protocols.

GST–NES^{Nup214} constructs [GST–Nup214 (878–887) and GST–Nup214 (878–887) L878A/L882A/L885A/L887A] and GST–Nup214 (1464–1473) were expressed in *E. coli* BL21(DE3) at 30°C for 4 h with 1 mM isopropyl-thio- β -D-galactoside (IPTG). Cells were harvested, washed with phosphate-buffered saline (PBS) and lysed in lysis buffer (50 mM Tris-HCl pH 6.8, 300 mM NaCl, 1 mM MgCl₂ and 1 mM DTT, supplemented with 1 μ g/ml each of aprotinin, leupeptin and pepstatin and 100 μ M PMSF) using an EmulsiFlex-C3 (Avestin, Mannheim, Germany). Lysates were cleared by centrifugation at 100,000 *g* at 4°C for 30 min, and the supernatant was added to 50 ml tubes containing Glutathione Sepharose 4 Fast Flow resin (GE Healthcare), equilibrated in lysis buffer. The lysate was rotated at 4°C for 45 min, the beads were washed three times with 45 ml lysis buffer, and bound proteins were eluted with lysis buffer supplemented with 15 mM glutathione. Glutathione was removed with PD-10 columns (GE Healthcare) equilibrated in lysis buffer, and proteins were flash frozen in liquid nitrogen and stored in aliquots at –80°C.

MBP–Nup214–His fragments were expressed in *E. coli* BL21(DE3) codon⁺ and grown in LB medium supplemented with 10% glycerol to an OD₆₀₀ of 0.6 at 37°C. The culture was cooled to 16°C, and protein expression was induced with 0.2 mM IPTG overnight at 16°C. Cells were harvested at an OD₆₀₀ of 1–2, lysed in lysis buffer [20 mM HEPES, pH 8.0, 100 mM KCl, 10 mM Mg(OAc)₂, 10% glycerol, 0.01% TritonX-100 and 1 mM DTT, supplemented with 1 μ g/ml each of aprotinin, leupeptin, 1 μ M DTT, 1 μ M PMSF] and the lysate was cleared by centrifugation at 50,000 *g* at 4°C for 45 min. The supernatant was added to 50 ml tubes containing Ni-NTA agarose (QIAGEN) equilibrated in lysis buffer and rotated at 4°C for 1 h. The beads were washed three times with lysis buffer, and proteins were eluted in lysis buffer supplemented with 500 mM imidazole. Imidazole was removed with PD-10 columns (GE Healthcare) equilibrated in lysis buffer, and proteins were further purified by incubation with amylose beads (New England Biolabs) equilibrated in lysis buffer at 4°C for 1 h. The beads were washed three times with lysis buffer, and proteins were eluted in lysis buffer supplemented with 15 mM maltose, then dialyzed against lysis buffer overnight using a slide-A-lyzer (Thermo Fisher Scientific) before being flash frozen in liquid nitrogen and stored in aliquots at –80°C.

RanGAP assays

RanGAP assays were performed as described previously (Askjaer et al., 1999; Kehlenbach et al., 2001). Briefly, 500 nM CRM1 was incubated with 10 μ M Ran loaded with ³²P- γ -GTP and increasing concentrations of snurportin 1 or GST–Nup214–NES in transport buffer [20 mM HEPES, 1.1 mM KOAc, 2 mM Mg(OAc)₂ and 1 mM EGTA, pH 7.3]. GTP hydrolysis was initiated by the addition of 10 nM RanGAP. Reactions were stopped after 10 min by the addition of stop buffer (7% charcoal, 10% ethanol, 0.1 M HCl and 10 mM NaH₂PO₄) and analyzed by determining free radioactive phosphate. Results were normalized to a reaction without RanGAP and plotted as percent of maximal GTP hydrolysis.

Fluorescence polarization assays

NES peptides of Nup214, PKI and HIV-1 Rev (LNHLVDSLQQLRLK, LSNELALKLAGLDIK and LQLPPLRLTLK, respectively) were synthesized by EMC (Tübingen, Germany). 6-Carboxyfluorescein (6-FAM) was attached to a lysine residue in the NES peptide sequence. The NES peptides (40 nM) were incubated with CRM1 in the absence or presence of 3 μ M RanQ69L (1–180) GTP in a total volume of 150 μ l of anisotropy assay buffer [20 mM Tris-HCl, pH 7.4, 130 mM NaCl and 2 mM Mg(OAc)₂ supplemented with 1 mM DTT and 0.005% digitonin (Calbiochem, San Diego, CA, US)]. Samples were incubated at 25°C for 30 min, and fluorescence polarization was measured using a FluoroMax 4 fluorometer (Horiba, Kyoto, Japan). Excitation and emission wavelengths were set to 470 and 520 nm, respectively. Competition experiments were performed by forming complexes in the presence of 100 nM CRM1, followed by addition of increasing concentrations of the competitors

(snurportin 1, GST–NES^{Nup214} and GST–NES^{Nup214} 4 \times -mutant). Fluorescence anisotropy values were plotted and fitted, and the dissociation constants (*K_d*) were calculated using OriginLab 2021 (OriginLab Corporation, Northampton, MA, USA).

Gel filtration

His-tagged CRM1 and the fluorescently tagged NES^{Nup214} peptide (fNES^{Nup214}) were pre-incubated in 500 μ l of complex buffer [20 mM Tris-HCl, pH 7.4, 150 mM NaCl and 2 mM Mg(OAc)₂ supplemented with 1 mM DTT] on ice for 1 h either alone or in combination with RanQ69L (1–180) GTP or His–Nup214 (1916–2033), or both. All components were used at an equimolar ratio at a final concentration of 2 μ M each. After the pre-incubation, protein complexes were analyzed by gel filtration using a Superdex 200 10/300 GL analytical column (GE Healthcare), collecting 500 μ l fractions. For detection of the fNES^{Nup214} signal, 200 μ l of the eluted fractions were transferred to a 96-well plate and analyzed using a CLARIOstar Plus plate reader (BMG labtech, Ortenberg, Germany). The remaining proteins were precipitated using three volumes of ice-cold acetone. The resulting protein pellet was resuspended in 4 \times SDS sample buffer and analyzed by SDS–PAGE.

Pulldowns

GST- or MBP-fusion proteins (100 pmol) were immobilized on Glutathione Sepharose (GE Healthcare, Chicago, IL, USA) or amylose resin (New England Biolabs, Ipswich, MA, USA), respectively, equilibrated in binding buffer (50 mM Tris-HCl, pH 7.4, 200 mM NaCl, 1 mM MgCl₂ and 5% glycerol supplemented with 1 mM DTT and 20 mg/ml BSA). The beads were incubated with 100 pmol of purified proteins in a final volume of 500 μ l binding buffer for 6 h at 4°C and washed three times in binding buffer lacking BSA. Bound proteins were eluted in 4 \times SDS sample buffer and analyzed by SDS–PAGE followed by Coomassie staining.

Cell culture, plasmids and siRNA transfection

HeLa p4 (Charnau et al., 1994) cells and HEK 293T cells (CRL-3216, ATCC) were maintained in DMEM (Thermo Fisher Scientific, Waltham, MA, USA) supplemented with 10% (v/v) FBS Superior (Biochrom, Berlin, Germany), 100 μ g/ml streptomycin and 100 U/ml penicillin at 37°C and 5% CO₂. Cells were regularly tested to ensure absence of mycoplasma. For immunofluorescence experiments, cells were grown on coverslips overnight and transfected with the desired plasmids using the calcium chloride method (Chen and Okayama, 1987). For knockdown and re-expression experiments, cells were first transfected using Lipofectamine RNAiMAX (Thermo Fisher Scientific, Waltham, MA, USA) with siRNAs against Nup214 (5'-GUCACGAAACAGUGAAAG-3'; 20 nM; Sigma-Aldrich) or non-targeting control siRNA (20 nM; D-001810-01-50; Dharmacon, Lafayette, CO, USA). The next day, the proteins of interest were re-expressed by transfecting siRNA-resistant plasmids using the calcium chloride method. When needed, LMB (Enzo Life Sciences, Lörrach, Germany) was added to a final concentration of 10 nM from a 10 μ M stock in ethanol for 2 or 18 h. For hexanediol experiments, 5% 1,6-hexanediol (Sigma-Aldrich) in PBS was used.

Immunofluorescence and confocal microscopy

For immunofluorescence, the cells were washed, fixed with 3.7% formaldehyde in PBS and permeabilized using 0.5% Triton X-100 in PBS. Unspecific sites were blocked by incubating the coverslips with 30 mg/ml BSA in PBS for 30 min, followed by addition of primary antibodies diluted in PBS containing 10 mg/ml BSA for 1 h at room temperature. Coverslips were washed three times with PBS containing 10 mg/ml BSA, followed by incubation with fluorescently tagged secondary antibodies diluted in PBS containing 10 mg/ml BSA for 1 h at room temperature. Coverslips were washed with PBS and mounted using Mowiol (Sigma-Aldrich) mounting medium supplemented with 1 μ g/ml DAPI (Merck). Cells were analyzed using an LSM 510 meta confocal microscope (Zeiss, Oberkochen, Germany) with a 63 \times Plan-Neofluar 1.3 NA water-corrected objective, a TCS SP5 confocal microscope (Leica, Wetzlar, Germany) with a Leica HCX PL APO CS 63 \times /1.40–0.60 oil objective or a Nikon ECLIPSE Ti2 microscope with a 100 \times Plan-Apo

lambda 1.45 NA oil objective and proper filter settings. Images were processed using ImageJ and CellProfiler software (Kamentsky et al., 2011).

Immunoprecipitation

HEK 293T cells were seeded in 15 cm plates and grown until 50–60% confluency. Cells were transfected using the calcium chloride method. The cells were washed, harvested in NP40 buffer (50 mM Tris-HCl, pH 8.8, 150 mM NaCl and 1% NP40 supplemented with 1 mg/ml each of aprotinin, leupeptin, 1 μ M DTT and 1 μ M PMSF) and lysed on ice for 30 min. The lysate was cleared by centrifugation (16,000 *g* at 4°C for 30 min) and rotated with equilibrated magnetic GFP-trap beads (Chromotek, Planegg-Martinsried, Germany) at 4°C for 90 min. The beads were washed three times in NP40 buffer and suspended in 4 \times SDS sample buffer. The proteins were analyzed by SDS-PAGE followed by immunoblotting using appropriate antibodies, then visualized using an Odyssey Sa Infrared Imaging System (LI-COR, Bad Homburg, Germany).

Differential permeabilization and export assays

HeLa cells were seeded on coverslips and transfected with the appropriate plasmids via standard calcium chloride transfection. LMB was added as required. Cells were permeabilized with 0.007% or 1% digitonin (Calbiochem, San Diego, CA, USA) in transport buffer [20 mM HEPES, pH 7.3, 110 mM KOAc, 2 mM Mg(OAc)₂ and 1 mM EGTA] and fixed with 3.7% formaldehyde. Indirect immunostaining was performed as described above. Prior to export assays, cells were permeabilized using 0.007% digitonin in transport buffer. The coverslips were washed three times using transport buffer, transferred to a humid chamber at room temperature and then pre-incubated for 30 min with an ATP regenerating system [2000 U/ml creatine-kinase (CPK) enzyme, 80 mg/ml creatine phosphate and 100 mM ATP diluted in transport buffer]. Next, the cells were washed once with transport buffer and incubated with purified proteins for 30 min at room temperature. After the reaction, the cells were washed three times with transport buffer, fixed with 3.7% formaldehyde and mounted on glass slides.

Antibodies

For detection of protein tags, rabbit anti-GFP (Thermo Fisher Scientific, Waltham, MA, USA; A-11122; 1:1000) and mouse anti-myc antibody (Santa Cruz; SC-40; 1:200) were used. Endogenous proteins were detected by indirect immunofluorescence or immunoblotting using rabbit polyclonal anti-Nup214 antibody (Bethyl Laboratories, Montgomery, TX, USA; ICH-00103; 1:300), mouse monoclonal anti-Nup88 (BD Biosciences, Franklin Lakes, NJ, USA; 611896, 1:1000), mouse monoclonal antibody against nucleoporins (Mab414; BioLegend; MMS-120P; 1:5000), mouse monoclonal anti-Nup98 (Santa Cruz, Dallas, TX, USA; sc-74578; 1:100), rabbit polyclonal anti-Nup62 (Sigma-Aldrich, HPA005435; 1:1000), rabbit polyclonal anti-Nup153 (Sigma-Aldrich, HPA027896, 1:200), goat polyclonal anti-Nup358 (Frauke Melchior, Heidelberg; 1:1000), rabbit polyclonal anti-AHCTF1 (ELYS; Sigma-Aldrich; HPA031658; 1:500), rabbit polyclonal anti-Ran (ProteinTech, Manchester, UK; 10464-1-AP; 1:50), rabbit polyclonal anti-CRM1 (Kehlenbach et al., 1998; 1:3000), mouse monoclonal anti-lamin A/C (Abcam, Cambridge, UK; ab40567; 1:1000) and rabbit polyclonal anti-GAPDH (Proteintech, Rosemont, IL, USA; 10494-1-AP; 1:1000). For immunofluorescence, Alexa Fluor 594-conjugated donkey anti-mouse IgG, Alexa Fluor 555-conjugated goat anti-mouse IgG, Alexa Fluor 594-conjugated donkey anti-rabbit IgG, Alexa Fluor 488-conjugated donkey anti-rabbit IgG, Alexa Fluor 647-conjugated goat anti-rabbit IgG and Alexa Fluor 594-conjugated donkey anti-goat IgG (Molecular Probes, Eugene, OR, USA) were used as secondary antibodies at a dilution of 1:1000. For immunoblotting, IRDye 800CW donkey anti-rabbit IgM and IRDye 680CW donkey anti-mouse IgG1 (LI-COR, Bad Homburg, Germany) were used as secondary antibodies at a dilution of 1:10,000.

Image analysis

CellProfiler software (Kamentsky et al., 2011) was used to analyze confocal microscopy images. For quantification of fluorescence ratios, a pipeline was generated to measure the fluorescence signal intensities in the nucleus and

the cytoplasm. The DAPI channel was used to identify cell nuclei following a two-class Otsu adaptive thresholding strategy, setting the diameter of the nuclei to 50–400 pixels. The green channel was used to identify GFP objects, following an automatic thresholding strategy. Intensity values were used to distinguish clumped objects. The smoothing filter for de-clumping and the minimum allowed distance between local maxima were calculated automatically. The cell area was defined using the Distance-N method (Kamentsky et al., 2011), where the nuclear area was expanded by 80 pixels. The cytoplasm was defined by subtracting the nuclear area from the cell area. The intensity of the GFP signal was measured in the nucleus and the cytoplasm of each cell and the ratio of nucleus:cytoplasm signal intensity was calculated. Incomplete cells and cells touching the border of an image were excluded from the analysis.

Statistical analysis

Results are presented as mean \pm s.d. Statistical analyses were performed with GraphPad Prism software (GraphPad Software Inc., San Diego, CA, USA). *P* values were calculated from a one-way ANOVA with a Dunnett's post hoc test, and significance was defined as *P*<0.05.

Acknowledgements

We wish to thank Christiane Spillner and Ulrike Möller for technical support. We also thank Drs Gerard Grosveld, Ralf Ficner, Alaa Shaikhqasem and Dirk Görlich for the generous gift of reagents and Dr Christina James for comments on the manuscript.

Competing interests

The authors declare no competing or financial interests.

Author contributions

Conceptualization: R.H.K.; Methodology: M.H., B.C., S.A.P.; Formal analysis: M.H., B.C., S.A.P., R.H.K.; Investigation: M.H., B.C., S.A.P.; Data curation: M.H., B.C.; Writing - original draft: R.H.K.; Writing - review & editing: M.H., B.C., S.A.P.; Supervision: R.H.K.; Project administration: R.H.K.; Funding acquisition: R.H.K.

Funding

The work was funded by the Deutsche Forschungsgemeinschaft, Sonderforschungsbereich 860 (to R.H.K.).

Supplementary information

Supplementary information available online at <https://jcs.biologists.org/lookup/doi/10.1242/jcs.258095.supplemental>

Peer review history

The peer review history is available online at <https://jcs.biologists.org/lookup/doi/10.1242/jcs.258095.reviewer-comments.pdf>

References

- Ashkenazy-Titelman, A., Shav-Tal, Y. and Kehlenbach, R. H. (2020). Into the basket and beyond: the journey of mRNA through the nuclear pore complex. *Biochem. J.* **477**, 23–44. doi:10.1042/BCJ20190132
- Askjaer, P., Bachi, A., Wilm, M., Bischoff, F. R., Weeks, D. L., Ogniewski, V., Ohno, M., Niehrs, C., Kjems, J., Mattaj, J. W. et al. (1999). RanGTP-regulated interactions of CRM1 with nucleoporins and a shuttling DEAD-box helicase. *Mol. Cell. Biol.* **19**, 6276–6285. doi:10.1128/MCB.19.9.6276
- Bachi, A., Braun, I. C., Rodrigues, J. P., Pante, N., Ribbeck, K., von Kobbe, C., Kutay, U., Wilm, M., Görlich, D., Carmo-Fonseca, M. et al. (2000). The C-terminal domain of TAP interacts with the nuclear pore complex and promotes export of specific CTE-bearing RNA substrates. *RNA* **6**, 136–158. doi:10.1017/S1355838200991994
- Bastos, R., Ribas de Pouplana, L., Enarson, M., Bodoor, K. and Burke, B. (1997). Nup84, a novel nucleoporin that is associated with CAN/Nup214 on the cytoplasmic face of the nuclear pore complex. *J. Cell Biol.* **137**, 989–1000. doi:10.1083/jcb.137.5.989
- Baumhardt, J. M., Walker, J. S., Lee, Y., Shakya, B., Brautigam, C. A., Lapalombella, R., Grishin, N. and Chook, Y. M. (2020). Recognition of nuclear export signals by CRM1 carrying the oncogenic E571K mutation. *Mol. Biol. Cell* **31**, 1879–1891. doi:10.1091/mbc.E20-04-0233
- Belgareh, N., Snay-Hodge, C., Pasteau, F., Dagher, S., Cole, C. N. and Doye, V. (1998). Functional characterization of a Nup159p-containing nuclear pore subcomplex. *Mol. Biol. Cell* **9**, 3475–3492. doi:10.1091/mbc.9.12.3475
- Ben-Efraim, I., Frosst, P. D. and Gerace, L. (2009). Karyopherin binding interactions and nuclear import mechanism of nuclear pore complex protein Tpr. *BMC Cell Biol.* **10**, 74. doi:10.1186/1471-2121-10-74

- Bernad, R., van der Velde, H., Fornerod, M. and Pickersgill, H.** (2004). Nup358/RanBP2 attaches to the nuclear pore complex via association with Nup88 and Nup214/CAN and plays a supporting role in CRM1-mediated nuclear protein export. *Mol. Cell. Biol.* **24**, 2373-2384. doi:10.1128/MCB.24.6.2373-2384.2004
- Bernad, R., Engelsma, D., Sanderson, H., Pickersgill, H. and Fornerod, M.** (2006). Nup214-Nup88 nucleoporin subcomplex is required for CRM1-mediated 60 S preribosomal nuclear export. *J. Biol. Chem.* **281**, 19378-19386. doi:10.1074/jbc.M512585200
- Bischoff, F. R. and Görlich, D.** (1997). RanBP1 is crucial for the release of RanGTP from importin β -related nuclear transport factors. *FEBS Lett.* **419**, 249-254. doi:10.1016/S0014-5793(97)01467-1
- Bischoff, F. R. and Ponstingl, H.** (1991). Catalysis of guanine nucleotide exchange on Ran by the mitotic regulator RCC1. *Nature* **354**, 80-82. doi:10.1038/354080a0
- Bischoff, F. R., Krebber, H., Kempf, T., Hermes, I. and Ponstingl, H.** (1995a). Human RanGTPase-activating protein RanGAP1 is a homologue of yeast Rna1p involved in mRNA processing and transport. *Proc. Natl. Acad. Sci. USA* **92**, 1749-1753. doi:10.1073/pnas.92.5.1749
- Bischoff, F. R., Krebber, H., Smirnova, E., Dong, W. and Ponstingl, H.** (1995b). Co-activation of RanGTPase and inhibition of GTP dissociation by Ran-GTP binding protein RanBP1. *EMBO J.* **14**, 705-715. doi:10.1002/j.1460-2075.1995.tb07049.x
- Boer, J., Bonten-Surtel, J. and Grosveld, G.** (1998). Overexpression of the nucleoporin CAN/NUP214 induces growth arrest, nucleocytoplasmic transport defects, and apoptosis. *Mol. Cell. Biol.* **18**, 1236-1247. doi:10.1128/MCB.18.3.1236
- Brangwynne, C. P.** (2013). Phase transitions and size scaling of membrane-less organelles. *J. Cell Biol.* **203**, 875-881. doi:10.1083/jcb.201308087
- Charneau, P., Mirambeau, G., Roux, P., Paulous, S., Buc, H. and Clavel, F.** (1994). HIV-1 reverse transcription. A termination step at the center of the genome. *J. Mol. Biol.* **241**, 651-662. doi:10.1006/jmbi.1994.1542
- Chen, C. and Okayama, H.** (1987). High-efficiency transformation of mammalian cells by plasmid DNA. *Mol. Cell. Biol.* **7**, 2745-2752. doi:10.1128/MCB.7.8.2745
- D'Angelo, M. A., Anderson, D. J., Richard, E. and Hetzer, M. W.** (2006). Nuclear pores form de novo from both sides of the nuclear envelope. *Science* **312**, 440-443. doi:10.1126/science.1124196
- Dong, X., Biswas, A., Süel, K. E., Jackson, L. K., Martinez, R., Gu, H. and Chook, Y. M.** (2009). Structural basis for leucine-rich nuclear export signal recognition by CRM1. *Nature* **458**, 1136-1141. doi:10.1038/nature07975
- Doucet, C. M., Talamas, J. A. and Hetzer, M. W.** (2010). Cell cycle-dependent differences in nuclear pore complex assembly in metazoa. *Cell* **141**, 1030-1041. doi:10.1016/j.cell.2010.04.036
- Dultz, E. and Ellenberg, J.** (2010). Live imaging of single nuclear pores reveals unique assembly kinetics and mechanism in interphase. *J. Cell Biol.* **191**, 15-22. doi:10.1083/jcb.201007076
- Dultz, E., Zanin, E., Wurzenberger, C., Braun, M., Rabut, G., Sironi, L. and Ellenberg, J.** (2008). Systematic kinetic analysis of mitotic dis- and reassembly of the nuclear pore in living cells. *J. Cell Biol.* **180**, 857-865. doi:10.1083/jcb.200707026
- Engelsma, D., Bernad, R., Calafat, J. and Fornerod, M.** (2004). Supraphysiological nuclear export signals bind CRM1 independently of RanGTP and arrest at Nup358. *EMBO J.* **23**, 3643-3652. doi:10.1038/sj.emboj.7600370
- Fernandez-Martinez, J., Kim, S. J., Shi, Y., Upla, P., Pellarin, R., Gagnon, M., Chemmama, I. E., Wang, J., Nudelman, I., Zhang, W. et al.** (2016). Structure and function of the nuclear pore complex cytoplasmic mRNA export platform. *Cell* **167**, 1215-1228.e25. doi:10.1016/j.cell.2016.10.028
- Fischer, U., Huber, J., Boelens, W. C., Mattaj, L. W. and Lührmann, R.** (1995). The HIV-1 Rev activation domain is a nuclear export signal that accesses an export pathway used by specific cellular RNAs. *Cell* **82**, 475-483. doi:10.1016/0092-8674(95)90436-0
- Fontoura, B. M. A., Blobel, G. and Yaseen, N. R.** (2000). The nucleoporin Nup98 is a site for GDP/GTP exchange on ran and termination of karyopherin β 2-mediated nuclear import. *J. Biol. Chem.* **275**, 31289-31296. doi:10.1074/jbc.M004651200
- Fornerod, M., Boer, J., van Baal, S., Jaegle, M., von Lindern, M., Murti, K. G., Davis, D., Bonten, J., Buijs, A. and Grosveld, G.** (1995). Relocation of the carboxyterminal part of CAN from the nuclear envelope to the nucleus as a result of leukemia-specific chromosome rearrangements. *Oncogene* **10**, 1739-1748.
- Fornerod, M., Boer, J., van Baal, S., Morreau, H. and Grosveld, G.** (1996). Interaction of cellular proteins with the leukemia specific fusion proteins DEK-CAN and SET-CAN and their normal counterpart, the nucleoporin CAN. *Oncogene* **13**, 1801-1808.
- Fornerod, M., Ohno, M., Yoshida, M. and Mattaj, I. W.** (1997a). CRM1 is an export receptor for leucine-rich nuclear export signals. *Cell* **90**, 1051-1060. doi:10.1016/S0092-8674(00)80371-2
- Fornerod, M., van Deursen, J., van Baal, S., Reynolds, A., Davis, D., Murti, K. G., Fransen, J. and Grosveld, G.** (1997b). The human homologue of yeast CRM1 is in a dynamic subcomplex with CAN/Nup214 and a novel nuclear pore component Nup88. *EMBO J.* **16**, 807-816. doi:10.1093/emboj/16.4.807
- Franz, C., Walczak, R., Yavuz, S., Santarella, R., Gentzel, M., Askjaer, P., Galy, V., Hetzer, M., Mattaj, I. W. and Antonin, W.** (2007). MEL-28/ELYS is required for the recruitment of nucleoporins to chromatin and postmitotic nuclear pore complex assembly. *EMBO Rep.* **8**, 165-172. doi:10.1038/sj.embor.7400889
- Fried, H. and Kutay, U.** (2003). Nucleocytoplasmic transport: taking an inventory. *Cell. Mol. Life Sci.* **60**, 1659-1688. doi:10.1007/s00018-003-3070-3
- Gaik, M., Flemming, D., von Appen, A., Kastritis, P., Mücke, N., Fischer, J., Stelter, P., Ori, A., Bui, K. H., Baßler, J. et al.** (2015). Structural basis for assembly and function of the Nup82 complex in the nuclear pore scaffold. *J. Cell Biol.* **208**, 283-297. doi:10.1083/jcb.2014111003
- Grandi, P., Emig, S., Weise, C., Hucho, F., Pohl, T. and Hurt, E. C.** (1995). A novel nuclear pore protein Nup82p which specifically binds to a fraction of Nsp1p. *J. Cell Biol.* **130**, 1263-1273. doi:10.1083/jcb.130.6.1263
- Güttler, T., Madl, T., Neumann, P., Deichsel, D., Corsini, L., Monecke, T., Ficner, R., Sattler, M. and Görlich, D.** (2010). NES consensus redefined by structures of PKI-type and Rev-type nuclear export signals bound to CRM1. *Nat. Struct. Mol. Biol.* **17**, 1367-1376. doi:10.1038/nsmb.1931
- Hampel, B., Andres-Pons, A., Kastritis, P. and Beck, M.** (2019). Structure and assembly of the nuclear pore complex. *Annu. Rev. Biophys.* **48**, 515-536. doi:10.1146/annurev-biophys-052118-115308
- Hantschel, O., Wiesner, S., Güttler, T., Mackereth, C. D., Rix, L. L., Mikes, Z., Dehne, J., Görlich, D., Sattler, M. and Superti-Furga, G.** (2005). Structural basis for the cytoskeletal association of Bcr-Abl/c-Abl. *Mol. Cell* **19**, 461-473. doi:10.1016/j.molcel.2005.06.030
- Hutten, S. and Kehlenbach, R. H.** (2006). Nup214 is required for CRM1-dependent nuclear protein export in vivo. *Mol. Cell. Biol.* **26**, 6772-6785. doi:10.1128/MCB.00342-06
- Hutten, S. and Kehlenbach, R. H.** (2007). CRM1-mediated nuclear export: to the pore and beyond. *Trends Cell Biol.* **17**, 193-201. doi:10.1016/j.tcb.2007.02.003
- Kamentsky, L., Jones, T. R., Fraser, A., Bray, M.-A., Logan, D. J., Madden, K. L., Ljosa, V., Rueden, C., Eliceiri, K. W. and Carpenter, A. E.** (2011). Improved structure, function and compatibility for CellProfiler: modular high-throughput image analysis software. *Bioinformatics* **27**, 1179-1180. doi:10.1093/bioinformatics/btr095
- Katahira, J., Sträßer, K., Podtelejnikov, A., Mann, M., Jung, J. U. and Hurt, E.** (1999). The Mex67p-mediated nuclear mRNA export pathway is conserved from yeast to human. *EMBO J.* **18**, 2593-2609. doi:10.1093/emboj/18.9.2593
- Kehlenbach, R. H., Dickmanns, A. and Gerace, L.** (1998). Nucleocytoplasmic shuttling factors including Ran and CRM1 mediate nuclear export of NFAT in vitro. *J. Cell Biol.* **141**, 863-874. doi:10.1083/jcb.141.4.863
- Kehlenbach, R. H., Dickmanns, A., Kehlenbach, A., Guan, T. and Gerace, L.** (1999). A role for RanBP1 in the release of CRM1 from the nuclear pore complex in a terminal step of nuclear export. *J. Cell Biol.* **145**, 645-657. doi:10.1083/jcb.145.4.645
- Kehlenbach, R. H., Assheuer, R., Kehlenbach, A., Becker, J. and Gerace, L.** (2001). Stimulation of nuclear export and inhibition of nuclear import by a Ran mutant deficient in binding to Ran-binding protein 1. *J. Biol. Chem.* **276**, 14524-14531. doi:10.1074/jbc.M011087200
- Kindermann, B., Valkova, C., Krämer, A., Perner, B., Engelmann, C., Behrendt, L., Kritsch, D., Jungnickel, B., Kehlenbach, R. H., Oswald, F. et al.** (2019). The nuclear pore proteins Nup88/214 and T-cell acute lymphatic leukemia-associated NUP214 fusion proteins regulate Notch signaling. *J. Biol. Chem.* **294**, 11741-11750. doi:10.1074/jbc.RA118.006357
- Kirli, K., Karaca, S., Dehne, H. J., Samwer, M., Pan, K. T., Lenz, C., Urlaub, H. and Görlich, D.** (2015). A deep proteomics perspective on CRM1-mediated nuclear export and nucleocytoplasmic partitioning. *eLife* **4**, e11466. doi:10.7554/eLife.11466
- Kosugi, S., Hasebe, M., Tomita, M. and Yanagawa, H.** (2008). Nuclear export signal consensus sequences defined using a localization-based yeast selection system. *Traffic* **9**, 2053-2062. doi:10.1111/j.1600-0854.2008.00825.x
- Kraemer, D., Wozniak, R. W., Blobel, G. and Radu, A.** (1994). The human CAN protein, a putative oncogene product associated with myeloid leukemogenesis, is a nuclear pore complex protein that faces the cytoplasm. *Proc. Natl. Acad. Sci. USA* **91**, 1519-1523. doi:10.1073/pnas.91.4.1519
- Kroschwald, S., Maharana, S. and Simon, A.** (2017). Hexanediol: a chemical probe to investigate the material properties of membrane-less compartments. *Matters*, e201702000010. doi:10.19185/matters.201702000010
- Kudo, N., Wolff, B., Sekimoto, T., Schreiner, E. P., Yoneda, Y., Yanagida, M., Horinouchi, S. and Yoshida, M.** (1998). Leptomycin B inhibition of signal-mediated nuclear export by direct binding to CRM1. *Exp. Cell Res.* **242**, 540-547. doi:10.1006/excr.1998.4136
- Mackmull, M.-T., Klaus, B., Heinze, I., Chokkalingam, M., Beyer, A., Russell, R. B., Ori, A. and Beck, M.** (2017). Landscape of nuclear transport receptor cargo specificity. *Mol. Syst. Biol.* **13**, 962. doi:10.15252/msb.20177608
- Mahajan, R., Delphin, C., Guan, T., Gerace, L. and Melchior, F.** (1997). A small ubiquitin-related polypeptide involved in targeting RanGAP1 to nuclear pore complex protein RanBP2. *Cell* **88**, 97-107. doi:10.1016/S0092-8674(00)81862-0
- Matunis, M. J., Coutavas, E. and Blobel, G.** (1996). A novel ubiquitin-like modification modulates the partitioning of the Ran-GTPase-activating protein RanGAP1 between the cytosol and the nuclear pore complex. *J. Cell Biol.* **135**, 1457-1470. doi:10.1083/jcb.135.6.1457
- Mendes, A. and Fahrenkrog, B.** (2019). NUP214 in Leukemia: it's more than transport. *Cells* **8**, 76. doi:10.3390/cells8010076

- Monecke, T., Güttler, T., Neumann, P., Dickmanns, A., Görlich, D. and Ficner, R. (2009). Crystal structure of the nuclear export receptor CRM1 in complex with Snurportin1 and RanGTP. *Science* **324**, 1087-1091. doi:10.1126/science.1173388
- Nakielny, S., Shaikh, S., Burke, B. and Dreyfuss, G. (1999). Nup153 is an M9-containing mobile nucleoporin with a novel Ran-binding domain. *EMBO J.* **18**, 1982-1995. doi:10.1093/emboj/18.7.1982
- Napetschnig, J., Blobel, G. and Hoelz, A. (2007). Crystal structure of the N-terminal domain of the human protooncogene Nup214/CAN. *Proc. Natl. Acad. Sci. USA* **104**, 1783-1788. doi:10.1073/pnas.0610828104
- Napetschnig, J., Kassube, S. A., Debler, E. W., Wong, R. W., Blobel, G. and Hoelz, A. (2009). Structural and functional analysis of the interaction between the nucleoporin Nup214 and the DEAD-box helicase Ddx19. *Proc. Natl. Acad. Sci. USA* **106**, 3089-3094. doi:10.1073/pnas.0813267106
- Oka, M., Asally, M., Yasuda, Y., Ogawa, Y., Tachibana, T. and Yoneda, Y. (2010). The mobile FG nucleoporin Nup98 is a cofactor for Crm1-dependent protein export. *Mol. Biol. Cell* **21**, 1885-1896. doi:10.1091/mbc.e09-12-1041
- Oka, M., Mura, S., Yamada, K., Sangel, P., Hirata, S., Maehara, K., Kawakami, K., Tachibana, T., Ohkawa, Y., Kimura, H. et al. (2016). Chromatin-precursor Crm1 recruits Nup98-HoxA9 fusion to induce aberrant expression of Hox cluster genes. *eLife* **5**, e09540. doi:10.7554/eLife.09540
- Onischenko, E., Noor, E., Fischer, J. S., Gillet, L., Wojtynek, M., Vallotton, P. and Weis, K. (2020). Maturation kinetics of a multiprotein complex revealed by metabolic labeling. *Cell* **183**, 1785-1800.e26. doi:10.1016/j.cell.2020.11.001
- Ori, A., Banterle, N., Iskar, M., Andrés-Pons, A., Escher, C., Khanh Bui, H., Sparks, L., Solis-Mezarino, V., Rinner, O., Bork, P. et al. (2013). Cell type-specific nuclear pores: a case in point for context-dependent stoichiometry of molecular machines. *Mol. Syst. Biol.* **9**, 648. doi:10.1038/msb.2013.4
- Otsuka, S. and Ellenberg, J. (2018). Mechanisms of nuclear pore complex assembly - two different ways of building one molecular machine. *FEBS Lett.* **592**, 475-488. doi:10.1002/1873-3468.12905
- Otsuka, S., Bui, K. H., Schorb, M., Hossain, M. J., Politi, A. Z., Koch, B., Eltsov, M., Beck, M. and Ellenberg, J. (2016). Nuclear pore assembly proceeds by an inside-out extrusion of the nuclear envelope. *eLife* **5**, e19071. doi:10.7554/eLife.19071
- Paraskeva, E., Izaurralde, E., Bischoff, F. R., Huber, J., Kutay, U., Hartmann, E., Lührmann, R. and Görlich, D. (1999). CRM1-mediated recycling of snurportin 1 to the cytoplasm. *J. Cell Biol.* **145**, 255-264. doi:10.1083/jcb.145.2.255
- Paulillo, S. M., Phillips, E. M., Koser, J., Sauder, U., Ullman, K. S., Powers, M. A. and Fahrenkrog, B. (2005). Nucleoporin domain topology is linked to the transport status of the nuclear pore complex. *J. Mol. Biol.* **351**, 784-798. doi:10.1016/j.jmb.2005.06.034
- Paulillo, S. M., Powers, M. A., Ullman, K. S. and Fahrenkrog, B. (2006). Changes in nucleoporin domain topology in response to chemical effectors. *J. Mol. Biol.* **363**, 39-50. doi:10.1016/j.jmb.2006.08.021
- Port, S. A., Monecke, T., Dickmanns, A., Spillner, C., Hofele, R., Urlaub, H., Ficner, R. and Kehlenbach, R. H. (2015). Structural and functional characterization of CRM1-Nup214 interactions reveals multiple FG-binding sites involved in nuclear export. *Cell Rep.* **13**, 690-702. doi:10.1016/j.celrep.2015.09.042
- Port, S. A., Mendes, A., Valkova, C., Spillner, C., Fahrenkrog, B., Kaether, C. and Kehlenbach, R. H. (2016). The oncogenic fusion proteins SET-Nup214 and sequestosome-1 (SQSTM1)-Nup214 form dynamic nuclear bodies and differentially affect nuclear protein and Poly(A)⁺ RNA export. *J. Biol. Chem.* **291**, 23068-23083. doi:10.1074/jbc.M116.735340
- Rasala, B. A., Orjalo, A. V., Shen, Z., Briggs, S. and Forbes, D. J. (2006). ELYS is a dual nucleoporin/kinetochore protein required for nuclear pore assembly and proper cell division. *Proc. Natl. Acad. Sci. USA* **103**, 17801-17806. doi:10.1073/pnas.0608484103
- Ribbeck, K. and Görlich, D. (2002). The permeability barrier of nuclear pore complexes appears to operate via hydrophobic exclusion. *EMBO J.* **21**, 2664-2671. doi:10.1093/emboj/21.11.2664
- Ribbeck, K., Lipowsky, G., Kent, H. M., Stewart, M. and Görlich, D. (1998). NTF2 mediates nuclear import of Ran. *EMBO J.* **17**, 6587-6598. doi:10.1093/emboj/17.22.6587
- Ritterhoff, T., Das, H., Hofhaus, G., Schröder, R. R., Flotho, A. and Melchior, F. (2016). The RanBP2/RanGAP1*SUMO1/Ubc9 SUMO E3 ligase is a disassembly machine for Crm1-dependent nuclear export complexes. *Nat. Commun.* **7**, 11482. doi:10.1038/ncomms11482
- Roloff, S., Spillner, C. and Kehlenbach, R. H. (2013). Several phenylalanine-glycine motifs in the nucleoporin Nup214 are essential for binding of the nuclear export receptor CRM1. *J. Biol. Chem.* **288**, 3952-3963. doi:10.1074/jbc.M112.433243
- Saito, S., Miyaji-Yamaguchi, M. and Nagata, K. (2004). Aberrant intracellular localization of SET-CAN fusion protein, associated with a leukemia, disorganizes nuclear export. *Int. J. Cancer.* **111**, 501-507. doi:10.1002/ijc.20296
- Saito, S., Cigdem, S., Okuwaki, M. and Nagata, K. (2016). Leukemia-associated Nup214 fusion proteins disturb the XPO1-mediated nuclear-cytoplasmic transport pathway and thereby the NF- κ B signaling pathway. *Mol. Cell. Biol.* **36**, 1820-1835. doi:10.1128/MCB.00158-16
- Savas, J. N., Toyama, B. H., Xu, T., Yates, J. R., III and Hetzer, M. W. (2012). Extremely long-lived nuclear pore proteins in the rat brain. *Science* **335**, 942. doi:10.1126/science.1217421
- Shaikhqasem, A., Dickmanns, A., Neumann, P. and Ficner, R. (2020). Characterization of inhibition reveals distinctive properties for human and *Saccharomyces cerevisiae* CRM1. *J. Med. Chem.* **63**, 7545-7558. doi:10.1021/acs.jmedchem.0c00143
- Snow, C. J., Dar, A., Dutta, A., Kehlenbach, R. H. and Paschal, B. M. (2013). Defective nuclear import of Tpr in Progeria reflects the Ran sensitivity of large cargo transport. *Jl Cell Biol* **201**, 541-557. doi:10.1083/jcb.201212117
- Strasser, A., Dickmanns, A., Schmidt, U., Penka, E., Urlaub, H., Sekine, M., Lührmann, R. and Ficner, R. (2004). Purification, crystallization and preliminary crystallographic data of the m3G cap-binding domain of human snRNP import factor snurportin 1. *Acta Crystallogr. D Biol. Crystallogr.* **60**, 1628-1631. doi:10.1107/S0907444904015380
- Tan, P. S., Aramburu, I. V., Mercadante, D., Tyagi, S., Chowdhury, A., Spitz, D., Shammis, S. L., Gräter, F. and Lemke, E. A. (2018). Two differential binding mechanisms of FG-nucleoporins and nuclear transport receptors. *Cell Rep.* **22**, 3660-3671. doi:10.1016/j.celrep.2018.03.022
- Thakar, K., Karaca, S., Port, S. A., Urlaub, H. and Kehlenbach, R. H. (2013). Identification of CRM1-dependent nuclear export cargos using quantitative mass spectrometry. *Mol. Cell. Proteomics* **12**, 664-678. doi:10.1074/mcp.M112.024877
- Toyama, B. H., Arrojito e Drigo, R., Lev-Ram, V., Ramachandra, R., Deerinck, T. J., Lechene, C., Ellisman, M. H. and Hetzer, M. W. (2019). Visualization of long-lived proteins reveals age mosaicism within nuclei of postmitotic cells. *J. Cell Biol.* **218**, 433-444. doi:10.1083/jcb.201809123
- Vollmer, B., Lorenz, M., Moreno-Andrés, D., Bodenhöfer, M., De Magistris, P., Astrinidis, S. A., Schooley, A., Flötenmeyer, M., Leptihn, S. and Antonin, W. (2015). Nup153 recruits the Nup107-160 complex to the inner nuclear membrane for interphasic nuclear pore complex assembly. *Dev. Cell* **33**, 717-728. doi:10.1016/j.devcel.2015.04.027
- von Appen, A., Kosinski, J., Sparks, L., Ori, A., DiGiulio, A. L., Vollmer, B., Mackmull, M.-T., Banterle, N., Parca, L., Kastriitis, P. et al. (2015). In situ structural analysis of the human nuclear pore complex. *Nature* **526**, 140-143. doi:10.1038/nature15381
- von Lindern, M., Poustka, A., Lerach, H. and Grosveld, G. (1990). The (6;9) chromosome translocation, associated with a specific subtype of acute nonlymphocytic leukemia, leads to aberrant transcription of a target gene on 9q34. *Mol. Cell. Biol.* **10**, 4016-4026. doi:10.1128/MCB.10.8.4016
- von Lindern, M., Breems, D., van Baal, S., Adriaansen, H. and Grosveld, G. (1992a). Characterization of the translocation breakpoint sequences of two DEK-CAN fusion genes present in t(6;9) acute myeloid leukemia and a SET-CAN fusion gene found in a case of acute undifferentiated leukemia. *Genes Chromosomes Cancer* **5**, 227-234. doi:10.1002/gcc.2870050309
- von Lindern, M., Fornerod, M., van Baal, S., Jaegle, M., de Wit, T., Buijs, A. and Grosveld, G. (1992b). The translocation (6;9), associated with a specific subtype of acute myeloid leukemia, results in the fusion of two genes, dek and can, and the expression of a chimeric, leukemia-specific dek-can mRNA. *Mol. Cell. Biol.* **12**, 1687-1697. doi:10.1128/MCB.12.4.1687
- von Lindern, M., van Baal, S., Wiegant, J., Raap, A., Hagemeijer, A. and Grosveld, G. (1992c). Can, a putative oncogene associated with myeloid leukemogenesis, may be activated by fusion of its 3' half to different genes: characterization of the set gene. *Mol. Cell. Biol.* **12**, 3346-3355. doi:10.1128/MCB.12.8.3346
- von Moeller, H., Basquin, C. and Conti, E. (2009). The mRNA export protein DBP5 binds RNA and the cytoplasmic nucleoporin NUP214 in a mutually exclusive manner. *Nat. Struct. Mol. Biol.* **16**, 247-254. doi:10.1038/nsmb.1561
- Weberruss, M. and Antonin, W. (2016). Perforating the nuclear boundary - how nuclear pore complexes assemble. *J. Cell Sci.* **129**, 4439-4447. doi:10.1242/jcs.194753
- Wen, W., Meinkoth, J. L., Tsien, R. Y. and Taylor, S. S. (1995). Identification of a signal for rapid export of proteins from the nucleus. *Cell* **82**, 463-473. doi:10.1016/0092-8674(95)90435-2
- Wühr, M., Guttler, T., Peshkin, L., McAlister, G. C., Sonnett, M., Ishihara, K., Groen, A. C., Presler, M., Erickson, B. K., Mitchison, T. J. et al. (2015). The nuclear proteome of a vertebrate. *Curr. Biol.* **25**, 2663-2671. doi:10.1016/j.cub.2015.08.047
- Xu, D., Marquis, K., Pei, J., Fu, S.-C., Çağatay, T., Grishin, N. V. and Chook, Y. M. (2015). LocNES: a computational tool for locating classical NESs in CRM1 cargo proteins. *Bioinformatics* **31**, 1357-1365. doi:10.1093/bioinformatics/btu826